

to appear in the *Astronomical Journal*

## The Solar Neighborhood XIII: Parallax Results from the CTIOPI 0.9-m Program – Stars with $\mu \geq 1''0/\text{year}$ (MOTION Sample)

Wei-Chun Jao<sup>1</sup>, Todd J. Henry<sup>1</sup>, John P. Subasavage<sup>1</sup> and Misty A. Brown<sup>1</sup>

*Georgia State University, Atlanta, GA 30302-4106*

jao@chara.gsu.edu, thenry@chara.gsu.edu, subasavage@chara.gsu.edu,  
brown@chara.gsu.edu

Philip A. Ianna<sup>1</sup>, Jennifer L. Bartlett<sup>1</sup>

*University of Virginia, Charlottesville, VA 22903*

pai@virginia.edu, jlb2j@virginia.edu

and

Edgardo Costa<sup>1</sup>, René A. Méndez<sup>1</sup>

*Universidad de Chile, Santiago, Chile*

costa@das.uchile.cl, rmendez@das.uchile.cl

### ABSTRACT

We present the first set of definitive trigonometric parallaxes and proper motions from the Cerro Tololo Inter-American Observatory Parallax Investigation (CTIOPI). Full astrometric reductions for the program are discussed, including methods of reference stars selection, differential color refraction corrections, and conversion of relative to absolute parallax. Using data acquired at the 0.9-m at CTIO, full astrometric solutions and  $VRIJK_s$  photometry are presented for 36 red and white dwarf stellar systems with proper motions faster than  $1''0/\text{yr}$ . Of these, thirty three systems have the first ever trigonometric parallaxes, which comprise 41% of MOTION systems (those with proper motions greater than

---

<sup>1</sup>Visiting Astronomer, Cerro Tololo Inter-American Observatory. CTIO is operated by AURA, Inc. under contract to the National Science Foundation.

$1''/yr$ ) south of  $\delta = 0$  that have no parallaxes. Four of the systems are new members of the RECONS 10 pc sample for which the first accurate trigonometric parallaxes are published here: DENIS J1048-3956 ( $4.04 \pm 0.03$  pc), GJ 1128 (LHS 271,  $6.53 \pm 0.10$  pc), GJ 1068 (LHS 22,  $6.97 \pm 0.09$  pc), and GJ 1123 (LHS 263,  $9.02 \pm 0.16$  pc). In addition, two red subdwarf-white dwarf pairs, LHS 193AB and LHS 300AB, are identified. The white dwarf secondaries fall in a previously uncharted region of the HR diagram.

*Subject headings:* astrometry — stars: distance — photometry — solar neighborhood — stars: high proper motion stars — white dwarfs

## 1. Introduction

The first ever stellar trigonometric parallax was reported by F. Bessel in 1838 for 61 Cygni, after a “race” in which he narrowly defeated F. G. Wilhelm Struve and T. Henderson, who published the parallaxes for Vega and  $\alpha$  Centauri, respectively, in the next year. Since then, trigonometric parallax measurements have provided one of the most important parameters for understanding stellar astronomy — distance — and provide one of the sturdiest rungs on the cosmic distance ladder. Trigonometric parallaxes are used to derive the intrinsic luminosities of stars, calculate accurate masses for binary system components, and answer questions about stellar populations and Galactic structure. In addition, the solar neighborhood is mapped out via trigonometric parallaxes, and these nearby objects provide the brightest examples of many stellar types, supplying the benchmarks to which more distant stars are compared.

Two of the most important parallax references are the Yale Parallax Catalog (van Altena et al. 1995) and Hipparcos Catalog (ESA 1997). Combined, they offer  $\sim 120,000$  parallaxes both from space and ground observations. Of these, 92% of trigonometric parallaxes are from the Hipparcos mission. However, because of the relatively bright magnitude limit of Hipparcos, many nearby stars candidates were excluded. Consequently, the faint members of the solar neighborhood are under-presented, and these faint red, brown, and white dwarfs are the objects targeted by recent trigonometric parallax efforts, including the one discussed in this paper. Recent results for nearby red and brown dwarfs include the efforts of Ianna et al. (1996), Tinney et al. (1995, 2003), Dahn et al. (2002), and Vrba et al. (2004), which together have provided  $\sim 130$  total ground-based parallaxes since 1995.

## 2. The CTIOPI Effort and Sample

In order to recover “missing” members in the solar neighborhood, the Research Consortium On Nearby Stars (RECONS) group is currently carrying out a southern sky parallax survey known as Cerro Tololo Inter-American Observatory Parallax Investigation (CTIOPI). The primary goals of CTIOPI are to discover and characterize nearby red, brown, and white dwarfs that remain unidentified in the solar neighborhood. This program was selected as a NOAO Survey Program, and observations commenced in 1999 August. CTIOPI used both 0.9-m and 1.5-m telescopes during the NOAO Survey Program, and has continued on the 0.9-m as part of the SMARTS (Small and Moderate Aperture Research Telescope System) Consortium beginning in 2003 February. The RECONS team at Georgia State University is responsible for data reduction for the 0.9-m program, while data from the 1.5-m program is being analyzed by E. Costa and R. Méndez of the Universidad de Chile in Santiago. The extended 0.9-m program has recently surpassed 400 systems on the observing list, while the final 1.5-m program included  $\sim 50$  systems that were fainter (and for which less observing time was awarded).

Most of the target stars (hereafter, the “pi stars”) are selected for CTIOPI because available astrometric (e.g. high proper motion), photometric, or spectroscopic data indicate that they might be closer than 25 pc. In the 0.9-m program, roughly 95% of the pi stars are red dwarfs and the remainder are white dwarfs. The fainter brown dwarf candidates were included in the 1.5-m program. In all,  $\sim 30\%$  of the 0.9-m targets are members of what we call the MOTION sample — stellar systems having proper motions of at least  $1''/yr$ . This paper describes the first definitive astrometric results of CTIOPI, focusing on the results for 36 MOTION systems.

## 3. Observations

### 3.1. Astrometry Observations

The 0.9-m telescope is equipped with a  $2048 \times 2048$  Tectronix CCD camera with  $0''.401/\text{pixel}$  plate scale (Jao et al. 2003). All observations were made using the central quarter of the chip, yielding a  $6'.8$  square field of view, through  $V_J$ ,  $R_{KC}$  and  $I_{KC}$  filters (hereafter, the subscripts are not given)<sup>1</sup>. The dewar containing the CCD camera is mounted on the telescope with columns oriented in the north-south direction. A slight rotation relative to the

---

<sup>1</sup>Subscript: J = Johnson, KC = Kron-Cousins. The central wavelengths for  $V_J$ ,  $R_{KC}$  and  $I_{KC}$  are  $5475\text{\AA}$ ,  $6425\text{\AA}$  and  $8075\text{\AA}$ , respectively.

sky is possible because of instrument flexure and repositioning during telescope maintenance. This rotation angle can be calibrated, as discussed in section 4.1.

The observing procedures employed during CTIOPI mimic those used in University of Virginia southern parallax program at the Siding Spring Observatory in Australia, led by P. Ianna, who is a member of the CTIOPI team. When a star is observed for the first time, exploratory exposures are taken in the *VRI* filters to find a suitable set of reference stars in the field. The parallax filter and position of the field are selected to balance the brightness of the pi star with available potential reference stars, and that filter is used for all subsequent parallax frames. Because most of our pi stars are nearby star candidates, they are brighter than most of the field stars. We attempt to place the pi star on the chip so that 5 to 15 field stars of adequate flux can be included. Typically, a good reference star is not more than twice as bright as the pi star (in the few cases when the pi star is not the brightest star in the field), but has at least 1000 peak counts during a typical parallax exposure.

Bias frames and dome flats are taken at the beginning of each night to allow for basic data reduction calibration. Parallax observations are usually made within  $\pm 30$  minutes of a pi star's transit in order to minimize the corrections required for differential color refraction (DCR) corrections, which are discussed in section 4.2. A few faint pi stars are observed with a wider hour angle tolerance because frame acquisition takes longer. Exposure times for parallax frames typically provide a peak of  $\sim 50,000$  counts for the pi star (saturation occurs at 65,535 counts), in an effort to maximize the number of counts available for pi star and reference star centroiding. Usually, 3–10 frames are taken in each visit, depending primarily on the exposure time required. Multiple frames are taken to reduce the errors on the pi star and reference star positions at each observation epoch. The typical set of observations required to determine a final parallax and proper motion includes four seasons of observations carried out over at least 2.5 years (further details in section 6.1).

### 3.2. *VRI* Photometry Observations

The *VRI* photometry reported here was acquired at the CTIO 0.9-m utilizing the same instrument setup used for the astrometry frames. All of the results are from observations taken between November 1999 and September 2004. As with the astrometry observations, bias and dome flat images were acquired nightly and used for basic science frame calibration.

Most pi stars were observed at  $\sec z < 1.8$  or less (a few were between 1.8 and 2.0 airmasses because of extreme northern or southern declinations). Various exposure times were used to reach  $S/N > 100$  for pi stars in each of the *VRI* filters. Standard star fields

with averagely total 10 stars from Landolt (1992) and/or E-regions from Graham (1982) were observed several times each night to derive transformation equations and extinction curves. In addition, one or two very red standard stars with  $V - I > 3.7$  were observed in order to derive extinction coefficients for stars with a wide range of colors. Typically, a total of 4–5 standard star fields were observed 2–3 times each per night.

## 4. Astrometry Reductions

### 4.1. Initial Data Processing, Reference Star Selection, and Trail Plate Selection

The basic data reduction for the astrometry CCD frames includes overscan correction, bias subtraction and flat-fielding, performed using a customized IRAF package called *redpi* (because our pi stars are primarily red dwarfs). After processing the raw data, frames are sorted into storage directories by object until there are enough parallax frames and time coverage to derive a reliable astrometric solution, typically at least 40 frames over at least two years. When sufficient frames are available, *SExtractor* (Bertin & Arnouts 1996) is used to determine centroids for each pi star and a set of reference stars that is chosen using the following general guidelines:

1. A single frame is selected that was taken using the parallax filter. The seeing is required to be better than  $1''.5$  and images must have ellipticity less than  $\sim 20\%$ .
2. Five to 15 reference stars in the field are selected that evenly surround the pi star in order to determine reliable plate rotation, translation, and scaling coefficients.
3. Each reference star must have a complete set of  $VRI$  photometry, which is required for DCR corrections and the conversion of relative to absolute parallax.
4. Using the IRAF *imexam* task, each reference star is checked to make sure that it is not a resolved binary or galaxy.
5. Ideally, all of the reference stars are have peak counts above 1000, although some fields require the selection of fainter stars in order to have a sufficient number of reference stars.

After the first round of parallax reductions, each reference star is reexamined for a sizable parallax or proper motion, and removed from the reference field if necessary.

In order to calculate the parallax factors, accurate coordinates and a value for the Earth to Solar System barycenter distance need to be known. The coordinates used for parallax factor calculations are extracted from the Two Micron All Sky Survey (2MASS) All-Sky Point Source Catalog via OASIS. Because these objects are high proper motion stars, all of them were manually identified by comparison with finding charts instead of retrieving data blindly by setting a searching radius around a given RA and DEC. The coordinates listed in Table 2 for the pi stars have been shifted to epoch 2000 using available proper motion measurements, primarily Luyten (1979), instead of the epoch at which the images were taken by 2MASS. To compute an accurate distance from the Earth to the Solar System barycenter at the time of observation, the JPL ephemeris DE405 is used.

Before calculating the parallax and proper motion of the pi star using frames taken at many epochs, a single “trail plate” is selected as a fundamental reference frame to which all other images are compared. This trail plate is used to remove any rotation, translation, and scaling changes between frames. A customized program organizes the set of frames used during the reductions for a particular field, is run to calculate the hour angle, parallax factors, and FWHM of images for each frame, and a trail plate is selected using the results, using the following criteria:

1. All reference stars and pi star(s) have peak counts less than 65500 and greater than 100.
2. All reference stars and pi star(s) have ellipticity less than  $\sim 20\%$ .
3. All the reference stars and pi star(s) have FWHM less than  $2''.5$ . This criterion has been relaxed relative to the frame used for the initial selection of reference stars (when  $1''.5$  is the limit) in order for the trail plate to be nearly coincident with the meridian.
4. The hour angle is within 2 minutes of the meridian at the midpoint of the integration. A frame taken very near the meridian provides a trail plate with minimal DCR.

Usually, the definitive trail plate is the one having the smallest hour angle and best seeing of the frames available.

The rotation angle of the trail plate is calculated relative to the Guide Star Catalog 2.2 (GSC2.2) using WCSTools/imwcs<sup>2</sup>. Our parallax images are usually deeper than GSC2.2, so stellar objects with apparent magnitudes brighter than 18.0 and FWHM smaller than  $2''.5$

---

<sup>2</sup>WCSTools is available at <http://tdc-www.harvard.edu/software/wcstools/>.

(but larger than  $0''.6$  to avoid centroiding on cosmic rays and bad pixels) are used. Once the rotation angle is determined, the parallax factors and centroids for all reference stars and pi stars on the trail plate are recalculated and used as the fundamental reference frame.

## 4.2. Differential Color Refraction Corrections

DCR corrections are required because the pi star and reference stars are not of identical color; therefore, their positions as seen from underneath Earth’s atmosphere shift relative to one another because of different, but calibrateable amounts of refraction. Although most of our parallax observations suffer minimal DCR because they are made within 30 minutes of the meridian, sometimes frames are taken far enough from the meridian that it is advantageous to make DCR corrections, e.g. for important targets observed in non-ideal observing seasons and in cases when the total number of available frames can be boosted by utilizing photometry frames taken in the parallax filter. Different observing and reduction methods used to measure DCR have been discussed by Monet et al. (1992), Tinney (1993), Stone (1996), and Stone (2002). Here we use both the theoretical methods proposed by Stone (1996) and the empirical methodology proposed by Monet et al. (1992) to measure DCR for the CTIOPI program, and to make final corrections during astrometric reductions.

DCR calibration observations for CTIOPI were made during four photometric nights in December 2002 using the 0.9-m telescope at CTIO. This is the identical combination of telescope, filters, and CCD camera used during the parallax program. Ten different fields spread from zenith to low altitude that contained blue ( $V - I = 0.57$ ) to red ( $V - I = 3.22$ ) stars were selected and observed through the  $V$ ,  $R$  and  $I$  filters. Ten fields were each observed up to five times per night through hour angles of  $\pm 4$  hours. Exposure times were chosen to be the same as used in the parallax program for each field so that the faintest reference stars could be analyzed for DCR. In total, 72 stars were included in the final DCR analysis. Although refraction is, in general, a function of temperature, pressure, and humidity, due to the stable observing conditions throughout this run, these factors can be ignored, as discussed in Monet et al. (1992) and Stone (2002).

In order to provide a zero point reference frame for the DCR calculation, one set of images must be taken when the field transits. In other words, there is no refraction in the RA direction, and we assign zero refraction in the DEC direction, when the hour angle is zero. The components of refraction in the RA and DEC directions,  $R_m Z_x$  and  $R_m Z_y$  respectively (where  $R_m$  is the mean refraction), are given by

$$(\alpha - \alpha') \cos \delta = \frac{R_m \sin HA \cos \phi}{\cos \zeta} = R_m \cos \phi \sin HA \sec \zeta = R_m Z_x \quad (1)$$

$$\delta - \delta' = R_m S \sin \phi \sec \delta (\sec \zeta - \sec(\phi - \delta)) = R_m Z_y, \quad (2)$$

where  $(\alpha, \delta)$  are the coordinates without atmospheric refraction and  $(\alpha', \delta')$  are the coordinates after atmospheric refraction. The angle  $\phi$  is the latitude of the observing site, HA is the hour angle of a given star and  $\zeta$  is its zenith distance. As discussed in Monet et al. (1992),  $S$  merely represents the sign of the declination term, i.e.  $S = 1$  if  $(\phi - \delta) \geq 0$  and  $S = -1$  if  $(\phi - \delta) < 0$ . These empirical measurements assume that  $R_m$  is a polynomial function of  $V - I$  color (see also Monet et al. (1992)). We have determined the  $V$ ,  $R$ , and  $I$  magnitudes for all 72 stars in the ten fields used to calculate the DCR so that each filter can be calibrated against the  $V - I$  color (thereby producing three sets of equations as shown in the next section).

### 4.3. The Final DCR Model for CTIOPI

The images taken for the DCR model were reduced in a manner identical to the parallax frames, as discussed in section 4.1. The three  $VRI$  frames having the smallest hour angle were selected as trail plates assumed to have no DCR. Plate constants are calculated using the GaussFit<sup>3</sup> program (Jefferys, Fitzpatrick & McArthur 1987). Six plate constants are derived so that field rotation, translation, and scaling can be removed (see section 4.4). We ignore any effects of source proper motion or parallax during the four nights of DCR observations because they are negligible on that time scale. Consequently, after calculating the plate constants, the only shifts in stellar centroids are because of atmospheric refraction. The amount of centroid shift from the trail plate in the X direction is a direct measure of the refraction, as represented by the quantity on the far left side of Equation 1. Monet et al. (1992) (see their Figure 2) showed that because the refraction in the Y direction has been defined as shown in Equation 2 (effectively removing any shift in the Y direction for zero hour angle), the X shift ( $R_m Z_x$ ) will have more variation than the Y shift ( $R_m Z_y$ ) when the hour angle is different from zero. Therefore, we concentrate on the RA direction to determine the empirical polynomial function for  $R_m$ .

To determine the functional form of  $R_m$ , first the hour angle and  $Z_x$  for every useful star in the ten DCR calibration fields are derived. Then, based on the centroid shift and

---

<sup>3</sup>This is a program for least squares and robust estimation that is available from the Hubble Space Telescope (HST) Astrometry Team <ftp://clyde.as.utexas.edu/pub/gaussfit/manual/>.



$Z_x$  for various stars observed during the observing run, the slope of  $R_m$  versus  $Z_x$  can be found. Figure 1 shows an example for LHS 158 and a reference star in the field. The field was observed from 1.47 hours east of the meridian to 3.71 hours west, including eight sets of  $VRI$  observations at different hour angles. A linear fit, whose slope is  $R_m$ , was made for each filter to each of the 72 stars selected in the ten fields in order to provide an ensemble of values,  $R_m$ , as a function of  $V - I$  color.

We set the zero point for DCR to be  $R_m = 0$  when  $V - I = 0$ , thereby defining a star of that color to show no DCR, while all other stars’ DCR is measured relative to that. The 0<sup>th</sup> order coefficient for each field is slightly different from the others because there is rarely a star with  $V - I = 0$  in a frame, but the offset can be computed by a least squares fit for a polynomial function to all stars that are present in a given field. By combining the  $R_m$  slopes and the  $V - I$  values for all 72 stars, we generate the plots in Figure 2, showing the empirical fits with solid curves.

The mean empirical DCR functions<sup>4</sup> for three different filters are given by:

$$\begin{aligned} R_{m,V} &= -0.0407(V - I) + 0.00941(V - I)^2, \\ R_{m,R} &= -0.0417(V - I) + 0.0482(V - I)^2 - 0.0245(V - I)^3 + 0.0036(V - I)^4, \\ R_{m,I} &= +0.0007(V - I). \end{aligned} \quad (3)$$

The theoretical curves for all three filters were also calculated using the model from Stone (1996) and are shown in Figure 2 as dashed lines<sup>5</sup>. A hypothetical field at DEC =  $-26$ , “observed” during a night with temperature  $T = 12^\circ C$  and 40% humidity was chosen to generate the model curves. These conditions are similar to those encountered during CTIOPI observations. Twelve stars with spectral types of A0 V to M5 V were selected for the model, and were “observed” at positions that were 0 to 3 hours from the meridian.

As expected, Figure 2 shows that  $I$  band has the least DCR of the three filters. In all three filters the average difference between the model and the empirical curve is always less than 6 mas for stars with  $V - I < 3.2$ . Because our DCR sample is deficient in very red stars, the difference between the empirical and theoretical curves increases at the red end of the  $R$  band calibration. Note that when the stellar color is redder than  $V - I = 2.6$ , stars observed

---

<sup>4</sup>Different orders of polynomial fits were calculated for each filters. The ones with reasonable slope and points distribution are given.

<sup>5</sup>The FORTRAN code used to generate the curves was kindly provided by M. Begam from the Siding Spring Observatory parallax project, led by P. Ianna.

through the  $R$  filter will actually experience more DCR than they will when observed through the  $V$  filter. This result can be explained because we are discussing “differential” color refraction among a set of stars. At a given position in the sky, the amount of refraction is caused primarily by two factors — how photons in a given filter bandpass are refracted by the Earth’s atmosphere, and how the number of photons changes within the bandpass, i.e. the slopes of the various stellar spectra. In the case of the  $VRI$  filters, the  $R$  filter has the largest amount of refraction for the reddest stars because both factors are important, whereas in the  $V$  band the slopes of the stellar spectra do not change much for very red stars, and in the  $I$  band, the atmosphere does not refract the photons significantly, regardless of a star’s color. Consequently, the DCR correction for each star can be made by obtaining its  $V$  and  $I$  photometry and applying Equation 1 to 3.

A valuable comparison of astrometry reductions is shown in Figure 3, in which results from two reductions are presented for the same data — one with and one without DCR corrections. A series of high hour angle measurements were taken in mid-2003 to test our DCR protocol. The effects of DCR corrections are clearly seen when comparing these two panels. In the case of no DCR corrections (the two plots on the left), the X direction residuals show a very deep “valley” and the Y direction residuals show a large scatter. After the DCR corrections are applied, the X residuals flatten out, and the Y residuals are reduced and more symmetric around zero. The standard deviations for X and Y residuals drop from 12.5 and 8.6 mas to 5.6 and 8.4 mas, respectively, when DCR corrections are made. The larger reduction in the X direction is expected because the differential refraction is more significant in the RA direction.

#### 4.4. Least Squares Reduction of Images Taken at Many Epochs

Once DCR corrections are incorporated into the data reduction pipeline, the positions of a pi star and a set of reference stars can be accurately computed for an ensemble of frames, with each frame in the ensemble being compared to the trail plate. The relationship between a frame and the trail plate is based on the measured positions of reference stars only (not the pi star). A new set of coordinates for each reference star is derived as a function of the trail plate coordinates and a set of constants:

$$\begin{aligned}\xi &= Ax + By + C, \\ \eta &= Dx + Ey + F,\end{aligned}\tag{4}$$

where  $(x, y)$  are the original coordinates of a reference star, A–F are the *plate constants*,

and  $(\xi, \eta)$  are the coordinates after the transformation. This six-constant model allows for a different scale in both the X and Y directions, compensates for different amounts of translation in both directions, and includes a correction for any instrument rotation. The higher order plate constants — radial distortion:  $Rx(x^2 + y^2)$ , coma:  $Smx$  (m is magnitude), and decentering distortion:  $P(x^2 + y^2)$  (Eichhorn 1974) — are not included in the current calculations because parallax results from our standard stars are within  $2\sigma$  of all other observations and no systematic differences are seen (discussed in section 6.1).

Analysis of the stellar path of the pi star must take into account both proper motion and parallax, but each reference star also experiences both motions on the sky. Because accurate proper motions and parallaxes are rarely known for reference stars, we assume that the reference grid has  $\sum_i \pi_i = 0$  and  $\sum_i \mu_i = 0$  (van Altena et al. 1986, Benedict et al. 1999). Hence, the set of constants for each frame outlined in Equation 4 above is expanded to include the reference star motions, resulting in an expanded set of equations:

$$\begin{aligned}
 \xi_1^t &= A^1 x_1^1 + B^1 y_1^1 + C^1 + \mu_{x1} T + \pi_1 P_{\alpha 1}, \\
 \xi_2^t &= A^1 x_2^1 + B^1 y_2^1 + C^1 + \mu_{x2} T + \pi_2 P_{\alpha 2}, \\
 \xi_3^t &= A^1 x_3^1 + B^1 y_3^1 + C^1 + \mu_{x3} T + \pi_3 P_{\alpha 3}, \\
 &\dots \\
 \xi_n^t &= A^1 x_n^1 + B^1 y_n^1 + C^1 + \mu_{xn} T + \pi_n P_{\alpha n},
 \end{aligned}
 \tag{5}$$

where superscripts indicate frame numbers, subscripts indicate the identification numbers of reference stars, the product  $\mu T$  is the star’s total proper motion relative to the date of the trail plate, the product  $\pi P$  is the parallax offset from the date of the trail plate ( $P_\alpha$  is the parallax factor in RA), and  $\xi_n^t$  represents the x coordinate for the trail plate. The plate constants,  $A$ ,  $B$ , and  $C$  can be calculated from these equations using least squares methods which are constrained by the conditions of reference star parallaxes and proper motions summing to zero. A similar set of equations is obtained for the y coordinate (plate constants  $D$ ,  $E$ , and  $F$  in Equation 4). After the plate constants and reference star values for  $\mu$  and  $\pi$  are acquired,  $\mu$  and  $\pi$  (and their errors) are computed for the pi star.

The least squares calculation is run using Gaussfit (discussed in section 4.3), which typically requires three iterations to minimize  $\chi^2$ . The image quality of each frame and the reliability of reference stars are determined using the results of the initial run of Gaussfit. At this stage, reference stars with high proper motion, large parallax, large centroid residuals, or high photometric parallax are deleted. Entire frames with high residuals are also removed. The Gaussfit program is then run again to derive the final pi star  $\mu$  and  $\pi$  values.

#### 4.5. Conversion from Relative Parallax to Absolute Parallax

What we have measured reflects the parallax of the pi star relative to the set of reference stars is the relative trigonometric parallax,  $\pi$ . As discussed in van Altena (1974) and van Altena et al. (1988), there are (at least) three different ways to convert this *relative parallax* to the *absolute parallax*, which is a measure of the true distance to the pi star — using statistical methods, spectroscopic parallaxes, or photometric parallaxes for the reference stars.

Statistical methods rely on a model of the Galaxy for the disk and halo. By adopting a Galactic model and knowing the apparent magnitudes and Galactic coordinates of the reference stars, parallaxes can be estimated for the reference stars. No reference star color information is used. For example, van Altena et al. (1988) concludes that faint halo stars have ( $14.5 < V < 15.5$ ) with a narrow distribution in their parallaxes for fields near the north Galactic pole. However, bright disk stars ( $10.5 < V < 11.5$ ) exhibit a wide range of parallaxes. Therefore, faint reference stars have smaller mean parallaxes and require a small correction for the relative to absolute parallax conversion, while brighter reference stars require larger corrections. As discussed in section 4.1, the reference stars chosen for CTIOPI are the brightest available in the pi star fields (in order to obtain better centroids), so we do not use a statistical methodology for the conversion of relative to absolute parallax.

Using spectroscopic parallaxes is arguably the most reliable method to determine the correction from relative to absolute parallax because the spectral type and luminosity class of every reference star are determined. This allows us to distinguish main sequence stars from giants and subdwarfs, and to apply correct  $M_V - color$  relations for each class of star. However, this method requires a significant amount of observing time, and is not practical for CTIOPI, in which several hundred stars with  $\sim 10$  reference stars each are observed.

Instead, we use the photometric parallax method to convert the pi star’s relative parallax to its absolute parallax.  $VRI$  magnitudes for the pi star and all reference stars have already been acquired for the DCR corrections, so the same data can be used to estimate a parallax of each reference star. However, because of the lack of information about the luminosity class of these stars, these corrections assume that all of the reference stars are main-sequence stars. Additional corrections for the contamination by giants or galactic reddening have not been included because such corrections are anticipated to be much smaller than the typical errors on the final parallaxes.

The fundamental relations between  $M_V$  and color used in CTIOPI are based on the sample of stars within 10 pc (Henry et al. 1997, 2004). Close multiple stars, subdwarfs, evolved stars, and stars with poor trigonometric parallaxes have been deleted from this sample to provide reliable  $M_V - color$  relations. Three different colors,  $V - R$ ,  $V - I$ , and

$R - I$ , are used to calculate the mean photometric parallax for each reference star. The error on the photometric parallax for an individual star is taken to be the average difference between the mean photometric parallax and the parallax from each color. The weighted mean photometric parallax of the entire set of reference stars is then calculated, and represents the final correction from relative to absolute parallax. The error in the final correction is determined from

$$\frac{err_1/\pi_1^{phot} + err_2/\pi_2^{phot} + \dots + err_n/\pi_n^{phot}}{n} \times \pi_{weighted-mean}, \quad (6)$$

where  $n$  is the number of reference stars,  $err$  is the photometric parallax error of each star and  $\pi_{weighted-mean}$  is the weighted mean photometric parallax of the ensemble of reference stars. We note that the mean absolute parallax correction for all 36 MOTION stars in Table 2 is  $1.47 \pm 0.17$  mas.

## 5. Photometry Reductions

The same *redpi* package discussed in section 4.1 is used to process the raw photometry data. Stars of interest, including pi stars, reference stars, and photometric standard stars, are tagged and enclosed in an aperture with a  $7''$  radius if there are no nearby background stars that might contaminate the photometry. A  $7''$  radius aperture was used for the standard stars in order to match the aperture typically used by Landolt (1992). After removing cosmic rays, the instrumental magnitude is determined by summing all of the counts for pixels falling in the aperture. In the few cases where a contaminating source is within the  $7''$  aperture, an aperture correction is performed. A sky annulus with  $20''$  inner radius and  $3''$  width was applied to calculate the sky background counts.

The transformation equation for apparent magnitude is

$$m_{standard} = m_{inst} + a_1 + a_2(AM) + a_3(color) + a_4(color)(AM), \quad (7)$$

where  $m_{inst}$  is the instrumental magnitude from *IRAF/DAOPHOT*,  $a_1$  through  $a_4$  are the transformation coefficients,  $color$  is the color term (which may have various permutations using *VRI* magnitudes),  $AM$  is the airmass and  $m_{standard}$  is the standard magnitude from Landolt (1992). The *IRAF/fitparam* task is used to compute these coefficients via a least squares method. To generate the final *VRI* magnitudes on the Johnson-Kron-Cousins system, the transformation equation is applied using a custom-made Perl task. The advantage of this Perl script over the *IRAF/evalfit* task is that the output file contains not only the

*VRI* apparent magnitudes, but image names, magnitude errors, and the date of data reduction. These output files are then concatenated into a large master photometry database for future access.

## 6. Parallax Results

### 6.1. Parallax Results for Calibration Stars

Seven parallax standard stars were selected to check the reliability of CTIOPI results. They were selected so that different parts of the sky were represented. All but one, LHS 1777, are within 10 pc and have final parallax determinations with more than 60 frames spanning more than 2.5 years.

The trigonometric parallax results for these stars from CTIOPI and other sources are shown in Table 1 and Figure 4. Note that all of the measured CTIOPI parallaxes are within  $2\sigma$  of all other observations, indicating that the current parallax pipeline, DCR corrections, and conversion from relative to absolute parallax produce reliable results. The final parallax error is a combination of many factors, including (1) the accuracy of the coordinates, (2) the quality of the reference star frame (brightness, distribution), (3) the accuracy of the (x,y) centroids, including any ellipticity caused by any close component (4) the total number of parallax images, (5) the time span of the available frame series, (6) the parallax factor coverage, (7) the DCR corrections, and (8) the correction of relative to final absolute parallax. The first three factors can not easily be modified after they are chosen. However, the number of observations, the duration of the frames series, and the parallax factor coverage, can be controlled and depend only on the resources, staffing, and stamina of the CTIOPI Team. At present, a pi star is generally considered “finished” when all of the following criteria are met<sup>6</sup>:

1. the relative parallax error is less than 3 mas
2. the pi star has been observed for 4 or more seasons (one season includes 2-3 months of observations)
3. the pi star has been observed for at least 2.5 years
4. there are at least 40 frames of the field

---

<sup>6</sup>Exceptions occur when the pi star is faint, when poor reference star configurations are available, or when a pi star is blended with a background source or close physical companion.

5. *VRI* photometry has been obtained for the field

In practice, an extended time span results in meeting most of these criteria, so it is perhaps the best single benchmark to be used to evaluate parallax errors for the entire survey. Figure 5 illustrates how time coverage affects the relative parallax error for 10 different stars within 10 pc (six are calibration stars and four are additional CTIOPI targets). Parallax reductions were executed using various subsets of the complete data sets (each star indicated with a different symbol). A few stars show only  $\sim 2$  mas error after only about one year of observations. In these cases, the parallaxes determined can be quite inaccurate, but a good fit with minimal formal error can be made to the proper motion and parallactic motion even though they have not yet been adequately decoupled. When key high parallax factor images are taken later, a different stellar path is determined and the error represents reality. The mean error for all of the reductions for all 10 fields is 2.45 mas. This error is reached at a time point 2.32 years into an observing sequence. We therefore conclude that  $\sim 2.5$  years of coverage is sufficient to determine accurate parallaxes with acceptable final errors based on the current time baseline we have. This is consistent with the results of Dahn et al. (2002), who find that the USNO parallaxes are stable after about 2 years observation.

### 6.2. Parallax Results for MOTION Stars

Complete astrometric results for 36 MOTION systems and the seven calibration stars are presented in Table 2. These are the first trigonometric parallaxes for 33 of the MOTION systems (GJ 545, GJ 754, and LHS 500/501 have improved parallaxes; see section 6.3 below). The first two columns are the identifiers and coordinates. The third column reports the filter used for parallax frames. The next four columns provide observational statistics.  $N_{sea}$  indicates the number of seasons observed, where 2-3 months of observations count as one season. The letter “c” indicates a continuous set of observations where multiple nights of data were taken in each season, whereas an “s” indicates scattered observations when some seasons have only a single night of observations. Generally, “c” observations are better. A + indicates that three or fewer individual images are used in one or more seasons that are not counted in  $N_{sea}$ .  $N_{frm}$  is the total number of frames used in the final reduction, and Years indicates the number of years spanned by the full reduction set.  $N_{ref}$  indicates the number of reference stars used during parallax reductions. Columns 8-10 report the relative parallax, size of the relative to absolute parallax correction, and the final absolute parallax, respectively. The next two columns are the proper motion and the direction of proper motion. The thirteenth column is the derived tangential velocity for each pi star. The last column has a “!” , if there are notes in section 6.3.

### 6.3. Notes on Individual Systems

Here we comment on individual systems that have ! in the notes column of Table 2.

**GJ 1050 (LHS 157)** The field lacks bright reference stars, so some reference stars with fewer than 100 peak counts are included, causing a relatively large parallax error of 4.44 mas. The photometric distance from the Henry et al. (2004) relations is  $14.9 \pm 2.2$  pc, which is comparable to our trigonometric parallax, thereby precluding any relatively bright unseen companion that may cause the high error.

**GJ 1068 (LHS 22)** is a new RECONS sample member at a distance of  $6.97 \pm 0.09$  pc. Ianna et al. (1994) reported a preliminary parallax of  $0''.1416 \pm 0''.0029$  (Ianna, 2004, private communication, not in print).

**LHS 193AB** is a new multiple system reported in Jao et al. (2003) with a separation of  $12''.6$ . A parallax has been determined only for LHS 193A because LHS 193B is too faint. The LHS 193AB system is a member of the MOTION sample based on the LHS catalog (Luyten 1979) value of  $\mu = 1''.023/\text{yr}$ , but Bakos, Sahu, & Németh (2002) flag this object as having a problematic proper motion. Our result of  $\mu = 0''.9964/\text{yr}$  indicates a proper motion slightly less than  $1''/\text{yr}$ . We now have a longer time base than given in Jao et al. (2003), but no orbital motion is detected. Reference star #3 (RA = 04 32 25.54, DEC =  $-39$  03 14.6, epoch = J2000.0) is relatively nearby, having  $\pi_{rel} = 0''.03054 \pm 0''.00168$ ,  $\mu = 0''.035/\text{yr}$ , and  $V - I = 2.71$ , and was dropped from the final reduction.

**LHS 225AB** is a multiple system reported in Jao et al. (2003) and also in NLTT Catalog (Luyten 1980) with a separation of  $2''.5$ . Parallaxes are determined for both components, but images with ellipticity greater than 20% had to be included during data reduction because of the proximity of the two sources. This causes both parallaxes to have relatively high errors.

**GJ 1123 (LHS 263)** is a new RECONS sample member at a distance of  $9.02 \pm 0.16$  pc. The spectroscopic and photometric distances estimated by Henry et al. (2002, 7.6pc) and Henry et al. (2004,  $7.5 \pm 1.2$  pc) are both with error less than 17% from this measurement.

**GJ 1128 (LHS 271)** is a new RECONS sample member at a distance of  $6.53 \pm 0.10$  pc, confirming the distance estimates of 6.6 pc in Henry et al. (2002) and  $6.4 \pm 1.0$  pc in Henry et al. (2004).

**GJ 1129 (LHS 273)** is a new NStars sample member at  $11.00 \pm 0.46$  pc, confirming the distance estimates of 11.6 pc in Henry et al. (2002). Images of the pi star are contaminated by a faint background star within a few arcseconds throughout the frame series, and blended during the last two epochs. This contamination causes the parallax residuals to have a "perturbation-like" curve resulting in a relatively large parallax error of 3.78 mas.



Nonetheless, the parallax result after the first 2.02 years matches the result after the full 4.27 years of the current dataset, so the result is reliable.

**DENIS J1048-3956** is a new RECONS sample member at a distance of  $4.04 \pm 0.03$  pc, confirming the distance estimate of  $4.5 \pm 0.7$  pc in Henry et al. (2004). Deacon & Hamby (2001) determined a trigonometric parallax of  $0''.192 \pm 0''.037$  using five SuperCOSMOS photographic plates. CTIOPI has improved the result to  $0''.24771 \pm 0''.00155$ <sup>7</sup>, making DENIS J1048-3956 the 28th nearest stellar system (after including two stars that are slightly closer for which we have preliminary, but as yet unpublished, parallax values).

**LHS 300AB** is a new multiple system reported in Jao et al. (2003) with a separation of  $4''.3$ . A mixture of resolved and unresolved images are included in the dataset, but because the B component is 4.9 mag fainter than A in the filter chosen for parallax frames,  $R$ , the centroid is not significantly corrupted by B.

**LHS 382** is close to the ecliptic, so the axis of the parallactic ellipse is small in the Y direction. Strong nebulosity is seen in this field.

**LTT 6933 (LHS 3292)** is a member of the MOTION sample based on the Bakos, Sahu, & Németh (2002) value of  $\mu = 1''.03/\text{yr}$  derived using POSS-I and POSS-II plates separated by 13.8 years. The LHS catalog reports  $\mu = 0''.996/\text{yr}$ , which is confirmed by our result of  $\mu = 0''.9593/\text{yr}$ .

**GJ 1226AB (LHS 263AB)** is a multiple system reported in Jao et al. (2003) and Vilkki (1984) with a separation of  $1''.4$ . Parallaxes were determined for both components. All 105 available frames were examined manually and only 59 images with good seeing were selected for data reduction. The absolute parallax correction for this field is over 5 mas and it is much larger than our mean corrections. Consequently, the mean correction 1.47 mas is adopted. Further investigation is necessary.

The Yale Parallax Catalog (van Altena et al. 1995) gives parallaxes for **GJ 545 (LHS 369)**,  $\pi_{trig} = 0''.0911 \pm 0''.015$ , **GJ 754 (LHS 60)**,  $\pi_{trig} = 0''.1752 \pm 0''.0101$ , and **LHS 500/501**,  $\pi_{trig} = 0''.075 \pm 0''.0171$ ). Our results have significantly improved the parallaxes by factors of 11, 7, and 11, respectively. LHS 500/501 is a wide binary with separation  $107''$  for which we have determined parallaxes for both components. The two parallaxes are entirely consistent, differing by  $1.8\sigma$ .

**Proxima Centauri (LHS 49)** is one of our parallax calibration stars. Proxima is brighter than the 0.9-m telescope limit in the  $I$  band, so  $VRI$  from Bessel (1990) has been

---

<sup>7</sup>The result from CTIOPI 1.5m (Costa et al. 2005) is  $0''.24978 \pm 0''.00181$

adopted for it, with proper transformations to the Johnson-Kron-Cousins system used for the calculation of the DCR corrections. The last epoch of data presented here (Dec 2003) was taken at an hour angle greater than 4 hours, so Stone’s (1996) theoretical model was used for DCR, rather than the empirical model. We note that our value of  $\pi_{trig} = 0''.77425 \pm 0''.00208$  is the most precise ground-based parallax ever determined for the nearest star to our Solar System, and has a formal error 13% smaller than the Hipparcos result.

## 7. *VRIJHK<sub>s</sub>* Photometry Results

The *VRIJHK<sub>s</sub>* photometry for the 48 stars in 43 systems is presented in Table 3. After the two names, the next four columns are the new optical *VRI* photometry and the number of new observations taken during CTIOPI. For comparison purposes, references for previously published photometry are listed in the seventh column. The next three columns are the infrared *JHK<sub>s</sub>* photometry (rounded to the hundredth) from 2MASS. Spectral types and references are given in the last two columns.

The *VRI* data have been reduced as discussed in section 3.2. Most of the stars are reduced using an aperture 7'' in radius. A few stars required smaller aperture sizes in order to separate two close components: LHS 193B (4''), LHS 225AB (2''), LHS 300AB (2''), and GJ 1226AB (1''). Errors from the fits of standard stars (external errors) are estimated to be  $\pm 0.02$  at *V*, *R* and *I*. Because most of the pi stars are bright, the signal to noise ratio errors (internal errors) are usually from 0.001 to 0.008 mag. The exceptions are LHS 193B (0.04, 0.05, 0.05 mag at *VRI*, respectively), DENIS 1048-3956 (0.02 at *V* band), and LHS 300B (0.01, 0.02, 0.02). We estimate that night-to-night repeatability errors for the faintest stars in the CTIOPI program (the worst case) are  $\sim 0.03$ , as discussed in Henry et al. (2004), except for those stars that are possibly variable, e.g. DEN 1048-3956. Thus, the combination of all three errors for the relatively bright stars presented here is typically  $\sim 0.03$  mag at *VRI*.

Infrared photometry in the *JHK<sub>s</sub>* system has been extracted from 2MASS. The *JHK<sub>s</sub>* magnitude errors from the total photometric uncertainties, including global and systematic terms, are almost always less than 0.05 mag and are typically 0.02-0.03 mag. The exceptions are LHS 193B (errors of 0.11, 0.16 and 0.18 at *JHK<sub>s</sub>*, respectively), LHS 271 (0.05 at *H*), Proxima Cen (0.06 at *H*) and LHS 3292 (0.06 at *H*).

## 8. Discussion

In this paper, the CTIOPI team presents the first substantial set of trigonometric parallaxes for stars with proper motion greater than  $1''0/\text{year}$  since the Yale Parallax Catalog and the Hipparcos mission. Hambly et al. (1999), Dahn et al. (2002), Tinney et al. (2003) and Vrba et al. (2004) have reported a total of 1, 1, 2 and 5 first trigonometric parallaxes for MOTION systems, respectively. All of those studies concentrated on the (very) cool end of main sequence, L or T dwarfs, or in a single case, a white dwarf. Obviously, the MOTION systems are potentially nearby stars, and this is borne out by our results — Table 2 shows that four of the systems are new entrants to the RECONS 10 pc sample, which requires a reliable trigonometric parallax published in a refereed journal for inclusion. Furthermore, 22 additional systems are new members of the NStars (25 pc) sample, and only seven systems lie beyond the NStars horizon. In sum, the first trigonometric parallaxes reported here for 33 MOTION systems provide reliable distances to 41% of the MOTION systems south of  $\delta = 0$  that previously had no trigonometric distance measurements.

The combination of accurate  $\pi_{trig}$  and  $VRIJK_s$  photometry permits the construction of reliable HR diagrams and offers the opportunity for insight into the MOTION sample. Here we present HR diagrams for the MOTION stars with new and improved parallaxes from CTIOPI, split into single-star systems and binaries (the parallax standard stars are not included in this discussion). In particular, we discuss the identification of new nearby subdwarfs, and two remarkable new K/M type subdwarf-white dwarf binaries (hereafter, sdK/M+WD).

### 8.1. HR Diagram for Single MOTION Stars

In Figure 6, we plot  $M_{K_s}$  against the  $V - K_s$  color for all stars in Table 3, excluding the parallax calibration stars and the five binary systems in the sample — LHS 193AB, LHS 225AB, LHS 300AB, LHS 500/501, and GJ 1226AB. These binaries will be discussed in the next section. Because of the high quality  $\pi_{trig}$  and  $VRIJK_s$  photometry, the errors in  $M_{K_s}$  and  $V - K_s$  are roughly the size of the symbols.

By comparing our sample with the main sequence stars from the RECONS 10 pc sample and subdwarfs from Gizis (1997), we can estimate the luminosity classes for several stars without spectral types. Of the 31 single MOTION stars, the seven labeled on the plot (and indicated with open circles) do not have spectral types. Three of these are new subdwarfs — LHS 158 at 40.1 pc, LHS 382 at 48.3 pc and LHS 521 at 46.3 pc. It is clear from Figure 6 that LHS 521 is an extreme subdwarf. The remaining four stars without spectral types are

main sequence stars that are all new NStars members — ER 2 at 11.9 pc, WT 1827 at 12.3 pc, pc LTT 6933 at 16.4 pc, and LHS 539 at 18.9 pc. Among the 24 stars with spectral types, three have been misclassified as main sequence stars, but are likely to be nearby subdwarfs — LHS 406 at 21.1 pc ( $M_{K_s} = 7.39$ ,  $V - K_s = 4.04$ ), WT 248 at 26.0 pc ( $M_{K_s} = 7.79$ ,  $V - K_s = 4.65$ ), and LHS 440 at 27.1 pc ( $M_{K_s} = 6.79$ ,  $V - K_s = 4.03$ ). Spectroscopic observations are necessary to confirm their luminosity classes.

This highly kinematically biased sample is of course likely to include Galactic thick disk members and even a few high velocity field halo subdwarfs. The tangential velocities of the new subdwarfs LHS 158 (191 km/sec), LHS 382 (327 km/sec), and LHS 521 (221 km/sec) are, indeed, quite high, implying that they belong to an old population. In order to analyze the full kinematics for these systems, future radial velocity observations are necessary.

## 8.2. HR Diagram for Binary MOTION Stars

Binary systems provide several opportunities to glean additional insight into stellar properties because the components are assumed to have formed simultaneously (so have the same age), and from the same gas cloud (so have identical composition). If parallaxes can be determined for both stars in a binary, a consistent match also indicates that our observing and reduction methodology is sound. The five binary systems in Tables 2 and 3 are shown on the  $M_V$  vs.  $V - I$  HR diagram in Figure 7.  $M_V$  has been used instead of  $M_{K_s}$  because  $K_s$  magnitudes are not available for the individual components in LHS 225AB, LHS 300AB, and GJ 1226AB. As discussed in the previous section, the RECONS and subdwarf samples are plotted for comparison, and have been supplemented in Figure 7 with white dwarfs from Bergeron, Leggett, & Ruiz (2001, hereafter, BLR).

It is clear from Figure 7 that the components of the close binaries LHS 225AB and GJ 1226AB are nearly identical main sequence M dwarfs. Our separate  $\pi_{trig}$  determinations for the components of the wide LHS 500/501 pair are consistent, and show that the two components are both main sequence M dwarfs.

The two remaining binaries, LHS 193AB and LHS 300AB, are both comprised of a subdwarf of late K/early M type and a white dwarf. A search of the literature indicates that few such systems are known. Gizis & Reid (1997) reported that LHS 2139/2140 is a common proper motion sdK/M+WD pair, based on a noisy but featureless spectrum for the B component, but no available parallaxes are available to confirm the nature of the system. Gizis (1998) argued that GJ 781AB, an unresolved spectroscopy binary, is another sdK/M+WD binary based on its mass function.

The two new wide sdK/M+ WD pairs reported here have complete parallax and  $VRI$  photometry. In both cases, Figure 7 clearly indicates that the primary star is a subdwarf and that the secondary is a white dwarf. However, both white dwarfs are redder than all white dwarfs with  $V - I$  and parallax reported in BLR. The locations of LHS 193B and LHS 300B in the HR diagram can possibly be explained several ways, including multiplicity, composition, very low mass (and hence large size), and/or dust.

In particular, models by Bergeron et al. (1995) indicate that very low mass helium white dwarfs may have the colors observed. Both Hansen (1998) and Bergeron (2001) argue that as the  $T_{eff}$  decreases to 3000 K for old ( $t \gtrsim 11$  Gyr) white dwarfs with hydrogen atmospheres, their location in the HR diagram swings back *blueward* of the white dwarf cooling sequence. This is caused by strong  $H_2$  molecular absorption features expanding into the optical regions. This implies that both LHS 193B and LHS 300B, which lie outside the grid for typical hydrogen white dwarfs, may be helium white dwarfs (or hydrogen white dwarfs with lower surface gravity values than have been included in the model grid – unlikely, because of the observed distribution of surface gravities for hydrogen white dwarfs). Very low S/N spectra currently in hand indicate that the two white dwarfs are featureless, in particular having no  $H\alpha$  line. Obviously, high S/N spectra are desirable, and will be the focus of future work.

## 9. Conclusions

Accurate  $\pi_{trig}$  and  $VRIJHK_s$  for nearby stars assist in constructing the basic framework of stellar astronomy. Here we provide a valuable contribution to studies of the solar neighborhood by targeting MOTION stars. A total of 46 parallaxes from CTIOPI are presented, including 39 parallaxes for 36 MOTION systems and 7 additional parallaxes for calibration stars. Thirty-three MOTION systems have trigonometric parallaxes determined for the first time.

Already, several new nearby systems have been revealed. Four of the MOTION systems — GJ 1068, GJ 1123, GJ 1128 and DENIS J1048-3956 — are new members of the RECONS 10 pc sample (Henry et al. 1997). An additional 22 systems are new members of the NStars 25 pc sample (Henry et al. 2003). In addition, valuable new nearby subdwarfs have been identified, and two rare sdK/M+WD pairs have been discovered. Both of these samples are valuable probes of the history of our Galaxy.

This work once again shows that faint, high proper motion stars are excellent candidates to discover nearby stars. Yet, 48 MOTION systems south of  $\delta = 0$  still do not have parallaxes.

In future papers, we will present  $\pi_{trig}$  and  $VRIJHK_s$  for several additional samples of stars, including more MOTION systems, stars neglected in the LHS Catalog, and new discoveries from our SuperCOSMOS RECONS search (Hambly et al. 2004, Henry et al. 2004, Subasavage et al. 2005), as well as others.

Finally, CTIOPI has been expanded in recent years under the SMARTS Consortium to carry out a program called ASPENS (Astrometric Search for Planets Encircling Nearby Stars), led by David Koerner at Northern Arizona University. Red and white dwarf systems within 10 pc south of  $\delta = 0$ , including the four new RECONS members and six of the seven calibration stars, are being observed intensely to reveal any possible long term astrometric perturbations.

## 10. Acknowledgments

We would like to thank Barbara McArthur, Mike Begam, Dave Monet, and Myles Standish for their assistance in building the data reduction pipeline. We gratefully acknowledge assistance in the early stages of the CTIOPI effort from Claudio Anguita, Rafael Pujals, Maria Teresa Ruiz and Pat Seitzer. Without the extensive observing support of Alberto Miranda, Edgardo Cosgrove, Arturo Gomez and the staff at CTIO, CTIOPI would not be possible. We also thank Jacob Bean, Thom Beaulieu, Charlie Finch, and Jennifer Winters for their assistance on data organization, reduction and observing. We thank Pierre Bergeron, John Gizis, Hugh Harris, Dave Latham, James Liebert, Hektor Monteiro, and Terry Oswalt for suggestions concerning the subdwarf-white dwarf binaries.

We are deeply indebted to NOAO for providing us a long term observing program at CTIO via the NOAO Surveys Project, using both the CTIO 0.9-m and 1.5-m telescopes. We also thank the continuing support of the members of the SMARTS Consortium without whom the completion of many astrometric series reported here would not have been possible. The early phase of CTIOPI was supported by the NASA/NSF Nearby Star (NStars) Project through NASA Ames Research Center. The RECONS team at Georgia State University is supported by NASA’s Space Interferometry Mission and GSU. This work has used data products from the Two Micron All Sky Survey, which is a joint project of the University of Massachusetts and the Infrared Processing and Analysis Center at California Institute of Technology funded by NASA and NSF.

EC and RAM acknowledge support by the Fondo Nacional de Investigación Científica y Tecnológica (proyecto Fondecyt No. 1010137), and by the Chilean Centro de Astrofísica FONDAP (No. 15010003). This project has made generous use of the 10% Chilean time.

## REFERENCES

- Bakos, G. Á., Sahu, K. C., & Németh, P. 2002, *ApJS*, 141, 187
- Benedict, G. F., et al. 1999, *AJ*, 118, 1086
- Bergeron, P., Wesemael, F., & Beauchamp, A. 1995, *PASP*, 107, 1047
- Bergeron, P., 2001, *ApJ*, 558, 369
- Bergeron, P., Leggett, S. K., & Ruiz, M. T. 2001, *ApJS*, 133, 413
- Bertin, E. & Arnouts, S. 1996, *A&AS*, 117, 393
- Bessel, M. S. 1990, *A&AS*, 83, 357
- Bidelman, W. P. 1985, *ApJS*, 59, 197
- Costa, E. et al, 2005, *AJ*, in preparation
- Dahn, C. C., et al. 2002, *AJ*, 124, 1170
- Deacon, N. R. & Hambly, N. C. 2001, *A&A*, 380, 148
- The *Hipparcos* and *Tycho* Catalogues, 1997, ESA SP-1200 (Noordwijk: ESA)
- Eichhorn, H., 1974, *Astronomy & of star positions; a critical investigation of star catalogues, the & methods of their construction, and their purpose*, Ungar, New York, 1974
- Gizis, J. E. 1997, *AJ*, 113, 806
- Gizis, J. E. & Reid, N.I., 1997, *PASP*, 109, 849
- Gizis, J. E. 1998, *AJ*, 115, 2053
- McCook, G. P., & Sion, E. M. 1999, *ApJS*, 121, 1
- Graham, J. A. 1982, *PASP*, 94, 244
- Harrington, R. S., et al. 1993, *AJ*, 105, 1571
- Hambly, N. C., et al. 1999, *MNRAS*, 309, L33
- Hambly, N. C., Henry, T. J., Subasavage, J. P., Brown, M. A., & Jao, W. 2004, *AJ*, 128, 437
- Hansen, Brad M. S. 1998, *Nature*, 394, 860

- Hawley, S. L., Gizis, J. E., & Reid, I. N. 1996, *AJ*, 112, 2799
- Henry, T. J., Backman, D. B., Blackwell, J., Okimura, T., & Jue, S. 2003, in *The Future of Small Telescopes In The New Millennium. Volume III — Science in the Shadows of Giants*, ed. T.D. Oswalt, Astrophysics and Space Science Library, Volume 289, Kluwer Academic Publishers, Dordrecht, 2003., p.111
- Henry, T. J., Kirkpatrick, J. D., & Simons, D. A. 1994, *AJ*, 108, 1437
- Henry, T. J., Ianna, P. A., Kirkpatrick, J. D., & Jahreiß, H. 1997, *AJ*, 114, 388
- Henry, T. J., Walkowicz, L. M., Barto, T. C., & Golimowski, D. A. 2002, *AJ*, 123, 2002
- Henry, T. J., Subasavage, J. P., Brown, M. A., Beaulieu, T. D., Jao, W., & Hambly, N. C. 2004, *AJ*, 128, 2460
- Ianna, P. A., Begam, M. C., & Mullis, C. R. 1994, *Bulletin of the American Astronomical Society*, 26, 1347
- Ianna, P. A., Patterson, R. J., & Swain, M. A. 1996, *AJ*, 111, 492
- Jao, W.-C, Henry, T. J., Subasavage, J. P., Bean, J. L., Costa, E., Ianna, P. A., & Méndez, R. A. 2003, *AJ*, 125, 332
- Jefferys, W. H., Fitzpatrick, M. J., & McArthur, B. E. 1987, *Celestial Mechanics*, 41, 39
- Landolt, A. U. 1992, *AJ*, 104, 340
- Luyten, W. J. 1979, *LHS Catalog*, Minneapolis, University of Minnesota, 1979, 2nd ed.
- Luyten, W. J. 1980, *NLTT Catalog*, Minneapolis, University of Minnesota, 1980
- Monet, D. G., Dahn, C. C., Vrba, F. J., Harris, H. C., Pier, J. R., Luginbuhl, C. B., & Ables, H. D. 1992, *AJ*, 103, 638
- Patterson, R. J., Ianna, P. A., & Begam, M. C. 1998, *AJ*, 115, 1648
- Tinney, C. G. 1993, *AJ*, 105, 1169
- Tinney, C. G., Reid, I. N., Gizis, J., & Mould, J. R. 1995, *AJ*, 110, 3014
- Tinney, C. G., Burgasser, A. J., & Kirkpatrick, J. D. 2003, *AJ*, 126, 975
- Stone, R. C. 1996, *PASP*, 108, 1051



Stone, R. C. 2002, PASP, 114, 1070

Subasavage, J. P., AJ, 2005, in press

van Altena, W. F. 1974, AJ, 79, 826

van Altena, W. F., Auer, L. H., Mora, C. L., & Vilkki, E. U. 1986, AJ, 91, 1451

van Altena, W. R. et al., "Parallax calibration of the population II main sequence, II. The effect of changes in the corrections to absolute parallax", , Calibration of stellar ages, 1988, Philip, A. G. D., 7, 175–184, Schenectady, N.Y.

van Altena, W. F., Lee, J. T., & Hoffleit, D. 1995, The General Catalogue of Trigonometric Stellar Parallaxes (4th ed.; New Haven: Yale Univ. Obs.)

Vilkki, E. U. 1984, PASP, 96, 161

Vrba, F. J., et al. 2004, AJ, 127, 2948

Weis, E. W. 1996, AJ, 112, 2300

Fig. 1.— This plot illustrates examples of atmospheric refraction shift for two stars having different colors. The slope for LHS 158 is  $-0.016$ , while the slope for field star #8 is  $+0.014$ . There is no point for field star #8 at  $Z_x \approx 0.02$  because of poor image quality.

Fig. 2.— These three plots illustrate the DCR data taken at the CTIO 0.9-m for ten parallax fields and the empirical least squares fits (solid lines) used in the final astrometric reductions for all three filters used in CTIOPI. The top panel is for the  $V$  filter, for which a second-order fit is used. The middle panel is for the  $R$  filter, for which a fourth-order fit is used. The bottom panel is for the  $I$  filter, for which a first-order fit is used. The curves from the theoretical models of Stone (1996) are plotted as dashed lines.

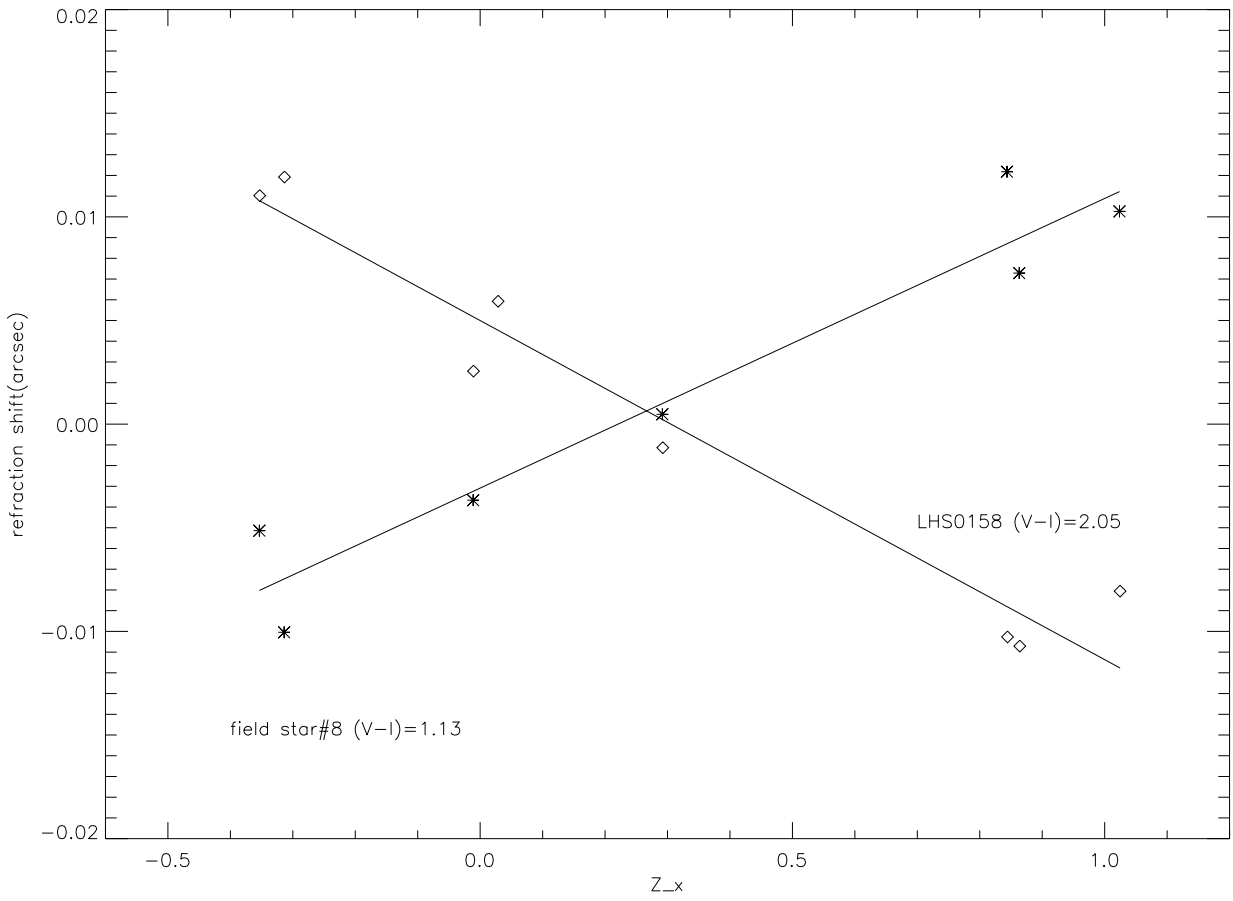
Fig. 3.— Effects of DCR corrections in the GJ 1061 field are illustrated for both the X and Y directions. These four plots indicate the X and Y residuals with (right two plots) and without (left two plots) DCR correction. The only images with HA greater than 100 mins are at the last epoch. The improvement in the X and Y residuals after DCR corrections is evident in the two plots in the right, especially in the X direction.

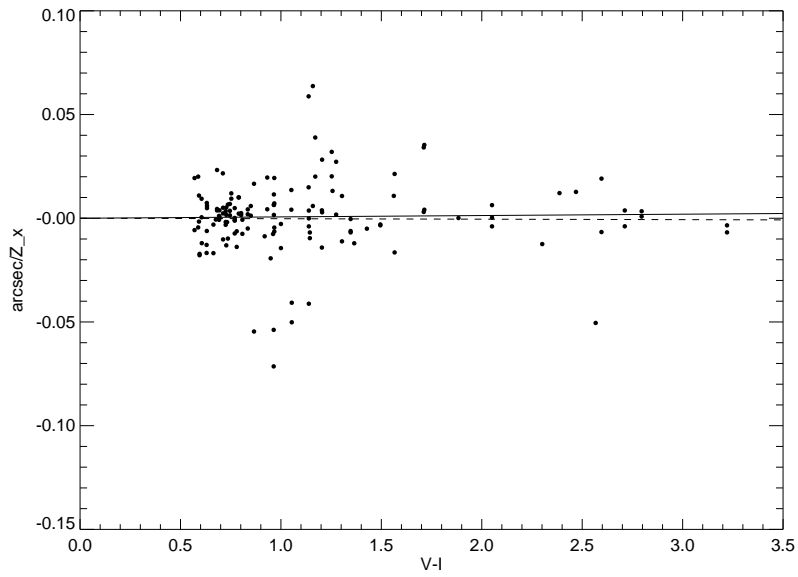
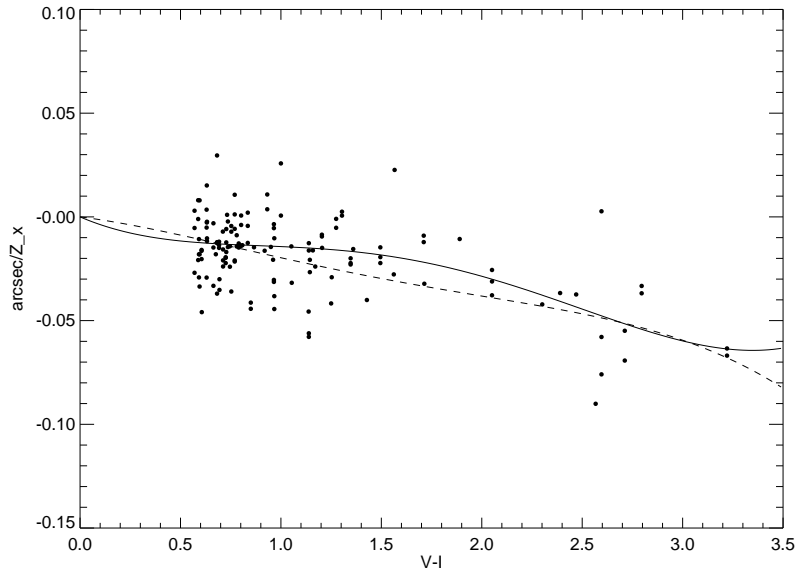
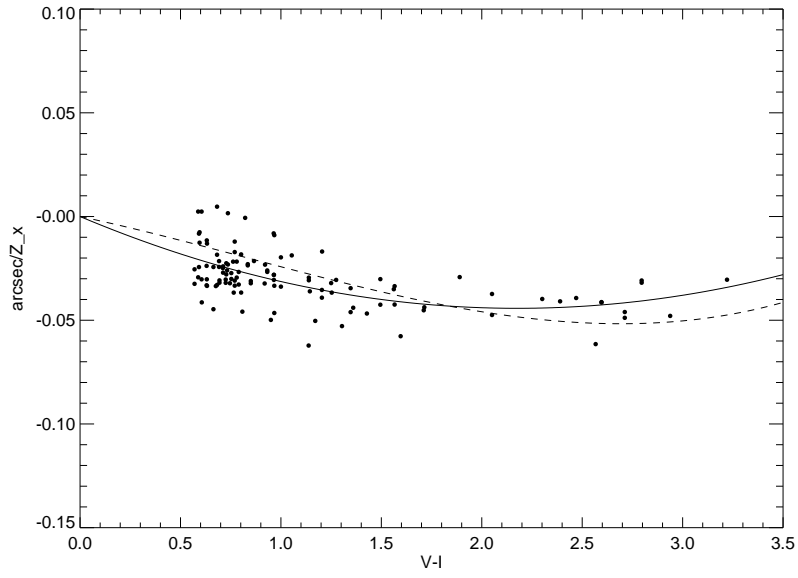
Fig. 4.— Comparison of CTIOPI parallaxes to parallaxes measured from the ground (YPC = Yale Parallax Catalog), and space (HIP = Hipparcos, HST = Hubble Space Telescope). Note that the CTIOPI parallaxes generally have errors smaller than those from YPC and comparable to those from HIP. The units on the Y axis are arcseconds.

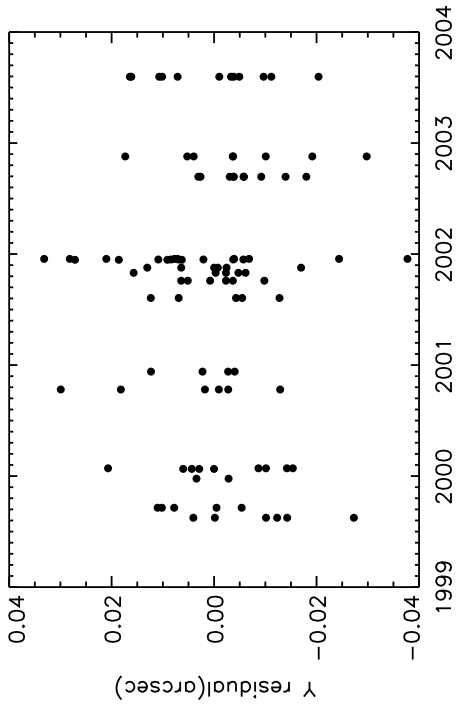
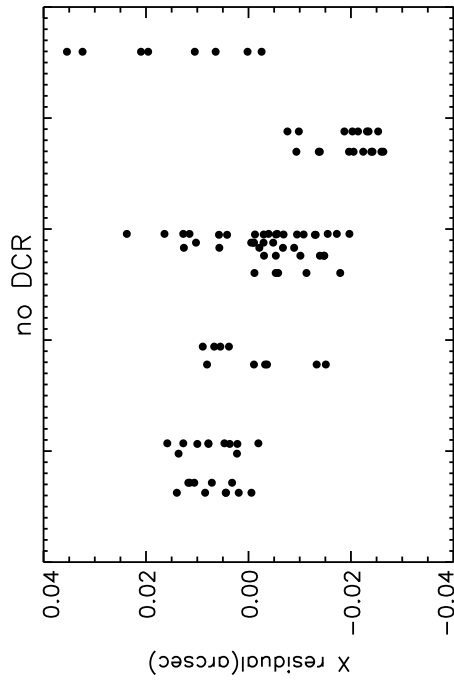
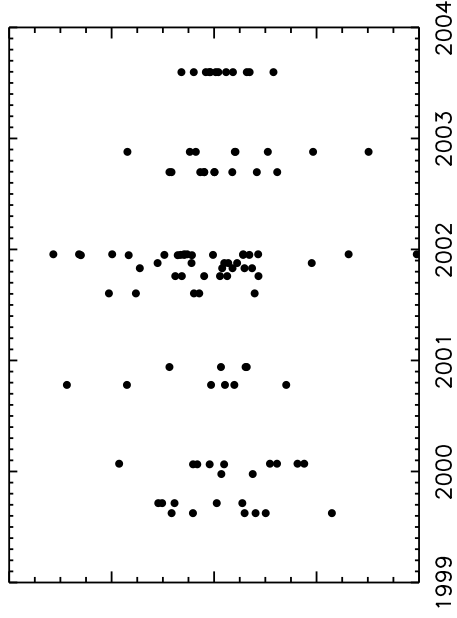
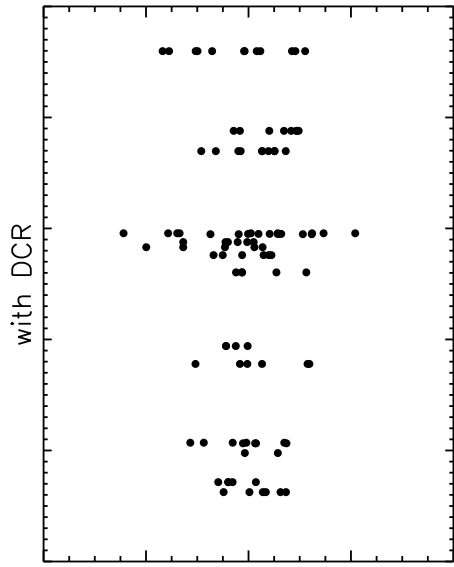
Fig. 5.— This plot shows the relation between relative parallax error and time coverage for 10 different nearby stars (each plotted using a different symbol). The dashed line indicates the mean error for all reductions of the 10 fields. The crossover point of the fit to the decreasing errors and the mean error for all reductions is at 2.32 years.

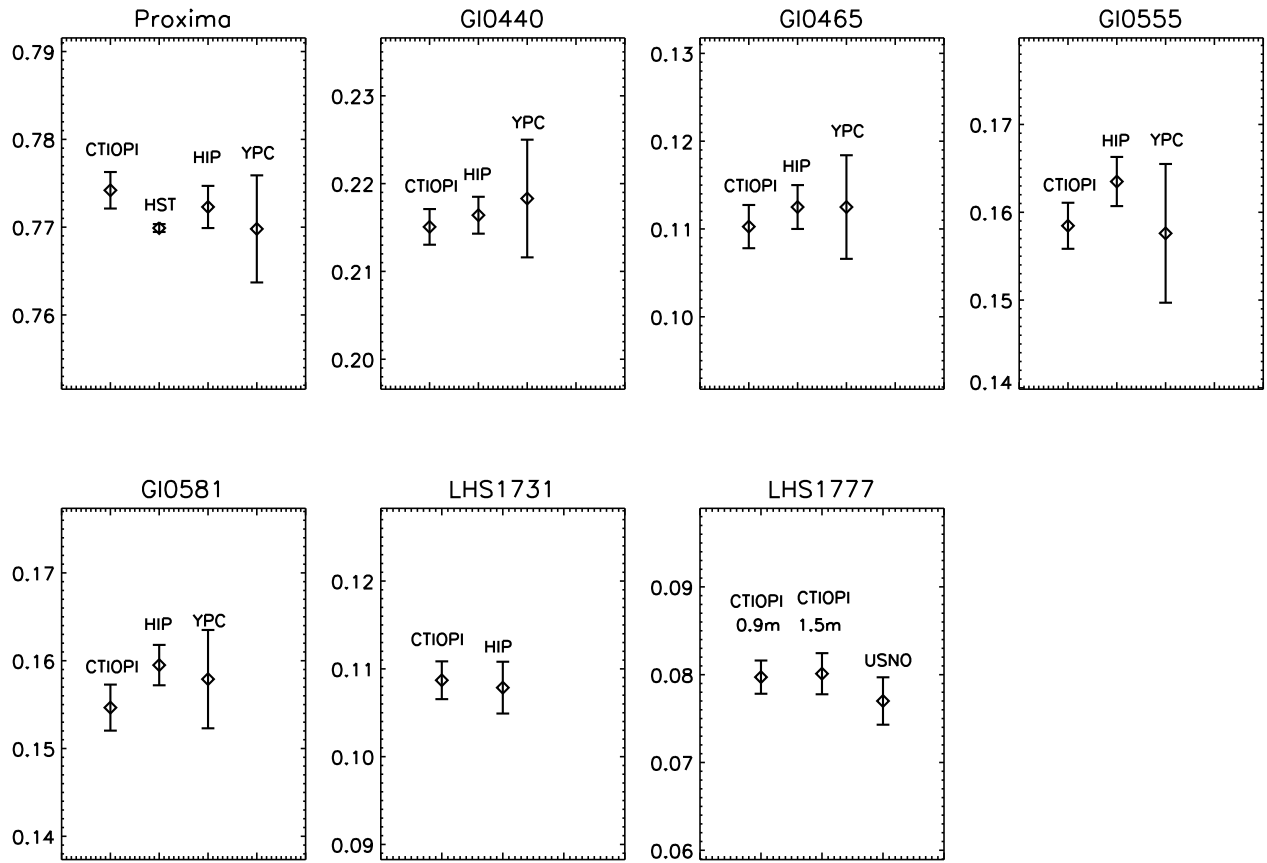
Fig. 6.— This HR diagram, using  $M_{K_s}$  vs.  $V - K_s$ , is shown for single MOTION stars with new and improved parallaxes. Filled circles represent 24 MOTION stars with published spectral types given in Table 3. Open circles represent 7 MOTION stars without spectral types. Open boxes represent 32 subdwarfs (LHS stars with  $\mu > 1''0/\text{yr}$ ) from Gizis (1997). Asterisks represent RECONS sample members and some very late M dwarfs discussed in Henry et al. (2004), with an empirical fit tracing the main sequence stars. The single solid point at the far right is DENIS J1048-3956.

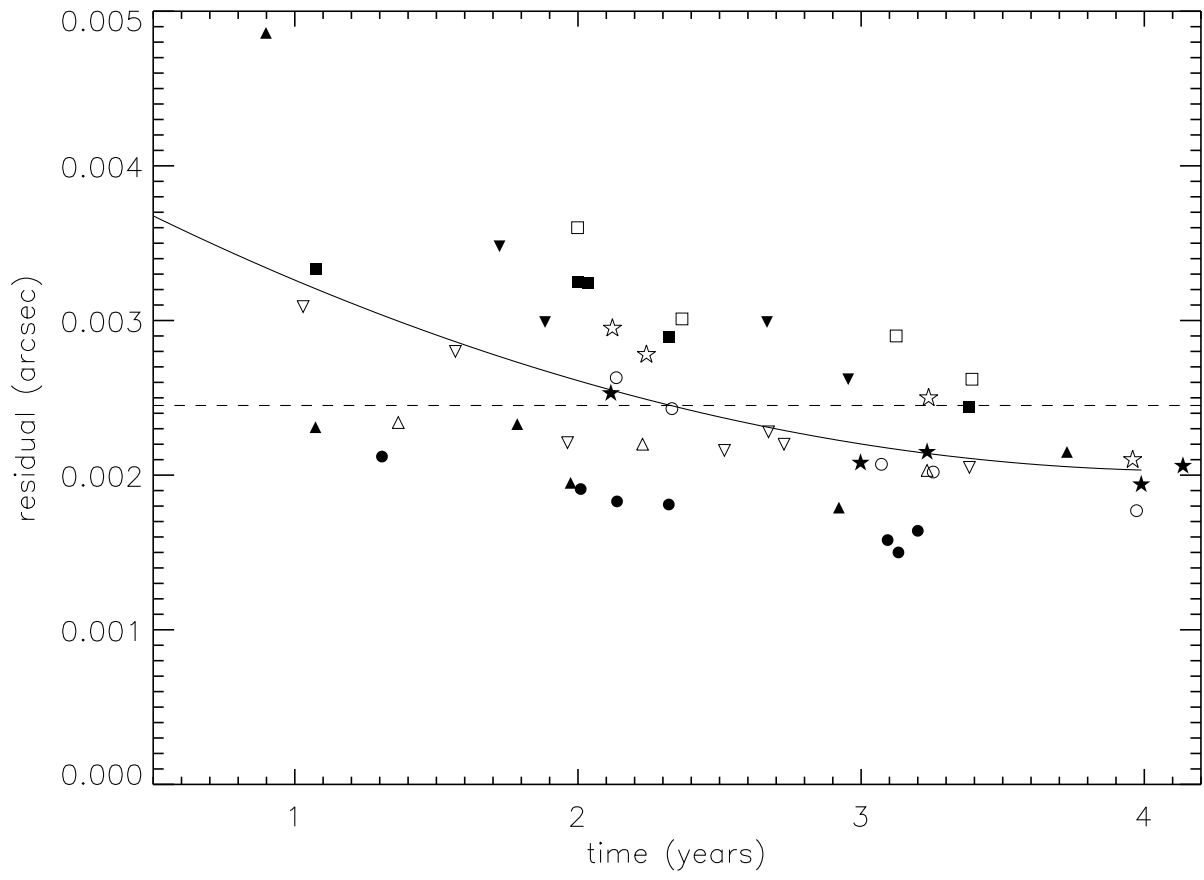
Fig. 7.— This HR diagram, using  $M_V$  vs.  $V - I$ , is shown for all components (solid points) in the five binary MOTION systems with new and improved parallaxes discussed in section 8.2. Symbols are the same as defined in Figure 6, supplemented with additional points for white dwarfs from BLR (open triangles are single white dwarfs, filled triangles are known or suspected double degenerates). The grid of models from Bergeron et al. (1995) outlines the extent of the hydrogen white dwarf sequence. The dotted line is for pure helium white dwarfs with  $\log g = 7$ , also from Bergeron et al. (1995). ESO 439-26 is a massive ( $1.19 M_\odot$ ), pure helium atmosphere white dwarf (BLR). LP 31-140 is a very low mass ( $0.19 M_\odot$ ) and low  $T_{eff}$  (4650 K) white dwarf (BLR). The error bars shown for the  $V - I$  colors of LHS 193B and LHS 300B are from the Poisson errors, whereas the errors in  $M_V$  are smaller than the filled circles.



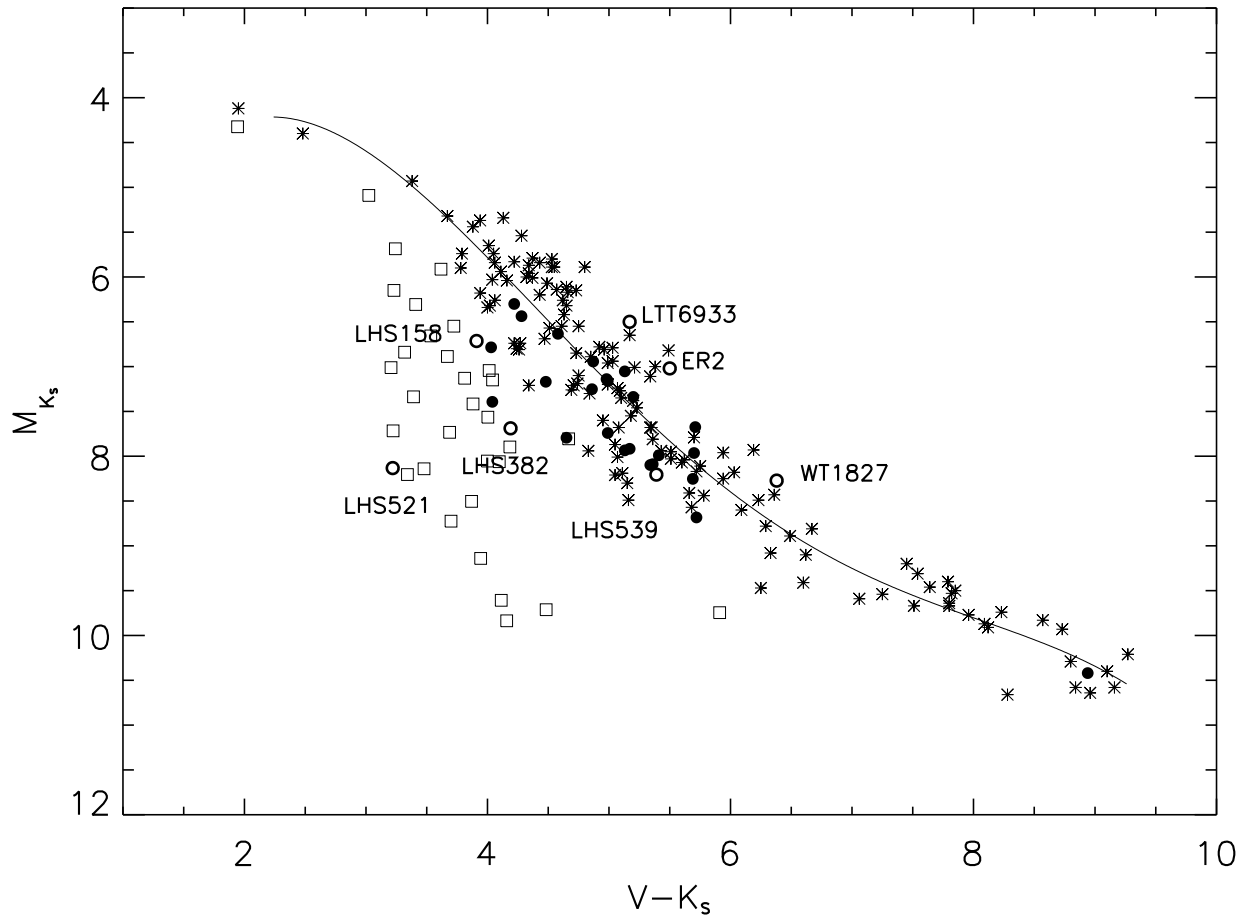












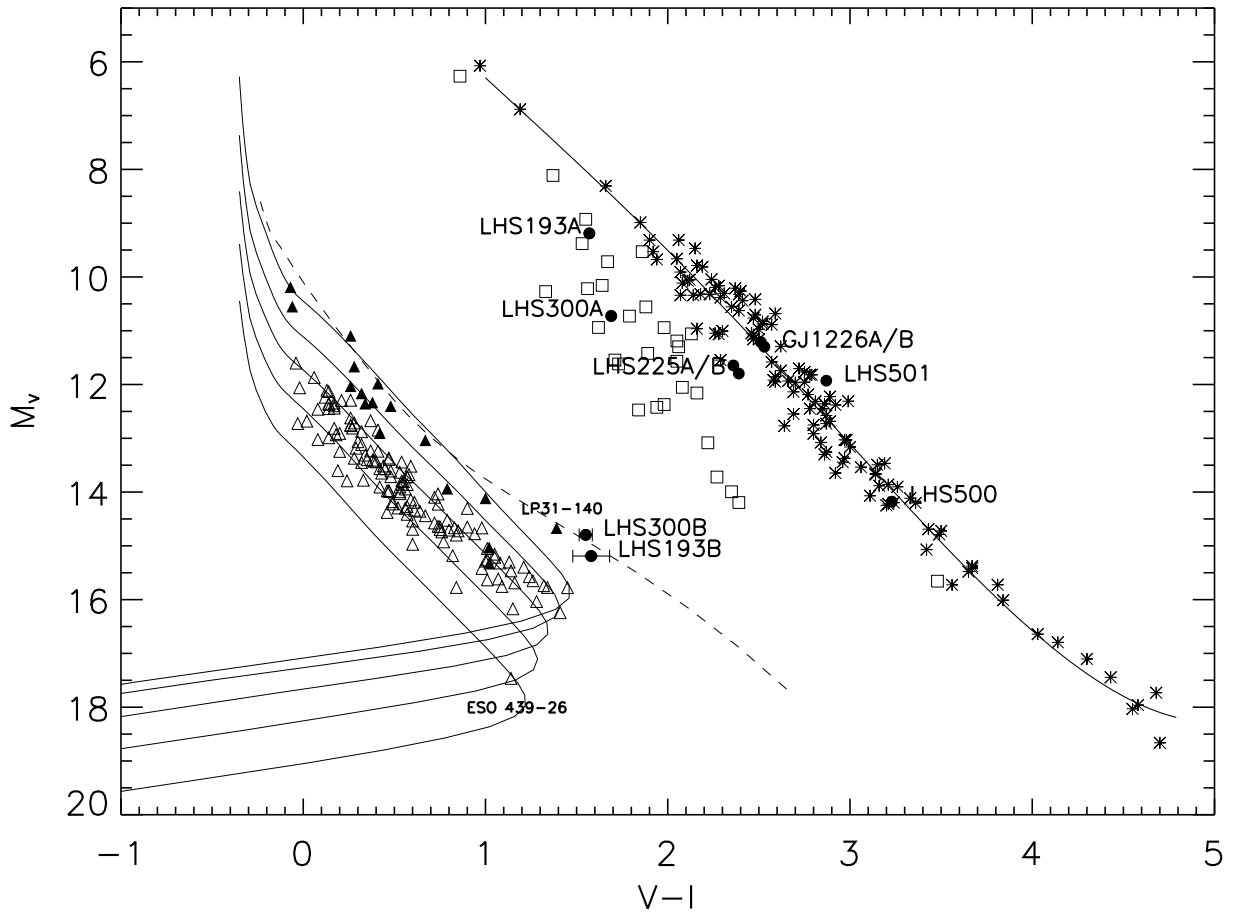


Table 1: The parallax standard stars from CTIOPI.

	CTIOPI	Hipparcos	YPC	others
Proxima <sup>a</sup>	0.77425±0.00208	0.77230±0.00240	0.76980±0.00610	0.76991±0.00054 <sup>b</sup>
GJ 440 <sup>a</sup>	0.21507±0.00204	0.21640±0.00210	0.21830±0.00670	...
GJ 465 <sup>a</sup>	0.11027±0.00246	0.11250±0.00250	0.11250±0.00590	...
GJ 555	0.15846±0.00262	0.16350±0.00280	0.15760±0.00790	...
GJ 581 <sup>a</sup>	0.15466±0.00262	0.15950±0.00230	0.15790±0.00560	...
LHS 1731	0.10870±0.00215	0.10786±0.00295	...	...
LHS 1777	0.07972±0.00189	...	0.07820±0.00270	0.08011±0.00234 <sup>c</sup>

---

Note. — The numbers indicate  $\pi \pm \text{error}$  in arcseconds.

<sup>a</sup>The star is a member of the MOTION sample.

<sup>b</sup>The parallax error from HST is slightly different from Benedict et al. (1999) because of improvement in the calculation of the correction from relative to absolute parallax (Benedict, 2003 private communication).

<sup>c</sup>The result is from CTIOPI 1.5-m (Costa et al. 2005)

Table 2.

Name	RA	DEC	Filt	Nsea	Nfrm	Years	Nref	$\pi$ (rel)	$\pi$ (corr)	$\pi$ (abs)	$\mu$	P.A.	$V_{tan}$	Note
(1)	(J2000.0)		(3)	(4)	(5)	(6)	(7)	(mas)	(mas)	(mas)	(mas/yr)	(deg)	(km/s)	(14)
First Trigonometric Parallaxes														
GJ 1025	01 00 56.37	-04 26 56.5	V	4c	46	3.28	7	87.13±2.38	0.57±0.05	87.70±2.38	1311.7±1.7	70.7±0.13	70.9	
GJ 1050	02 39 50.71	-34 07 57.5	V	4c	71	3.21	5	92.33±4.42	1.41±0.44	93.74±4.44	1736.9±3.9	162.5±0.23	87.8	!
LHS 158	02 42 02.88	-44 30 58.7	I	4c	84	2.91	10	23.23±1.61	1.71±0.12	24.94±1.61	1005.2±1.3	87.6±0.13	191.0	
GJ 1068	04 10 28.14	-53 36 08.2	R	5c	76	3.96	8	142.39±1.92	1.03±0.12	143.42±1.92	2553.5±1.6	199.1±0.06	84.4	!
LHS 193A	04 32 36.56	-39 02 03.4	V	4c	73	2.90	8	29.85±1.64	2.21±0.21	32.06±1.65	996.4±2.4	44.8±0.28	147.3	!
LHS 225B	07 04 45.77	-38 36 07.6	V	4c	74	3.29	9	52.10±3.83	1.96±0.10	54.06±3.83	1211.6±3.5	102.7±0.28	106.2	!
LHS 225A	07 04 45.77	-38 36 07.6	V	4c	74	3.29	9	54.95±2.67	1.96±0.10	56.91±2.67	1191.8±2.4	102.6±0.20	99.3	!
GJ 1118	08 59 05.31	-31 13 26.6	R	4c	60	3.18	11	54.78±1.76	1.41±0.11	56.19±1.76	1094.0±1.5	139.9±0.15	92.3	
GJ 1123	09 17 05.33	-77 49 23.4	V	4s	40	4.10	10	108.34±2.01	2.58±0.17	110.92±2.02	1051.7±2.1	141.6±0.23	44.9	!
GJ 1128	09 42 46.36	-68 53 06.0	V	3c+	71	4.10	11	151.45±2.40	1.60±0.24	153.05±2.41	1120.5±2.5	365.7±0.19	34.7	!
GJ 1129	09 44 47.34	-18 12 48.9	V	4s	55	4.27	8	89.23±3.78	1.70±0.13	90.93±3.78	1590.0±1.7	265.2±0.09	82.9	!
WT 248	10 05 54.94	-67 21 31.2	I	4c	52	3.95	11	37.32±2.83	1.12±0.08	38.44±2.83	1211.6±2.0	265.2±0.13	149.4	
LHS 281	10 14 51.77	-47 09 24.1	R	4c	60	3.19	10	82.45±1.69	0.62±0.03	83.07±1.69	1126.3±1.4	291.7±0.13	64.3	
WT 1827	10 43 02.81	-09 12 40.8	V	4c	65	4.14	8	80.47±2.42	0.52±0.10	80.99±2.42	1958.5±1.4	280.0±0.07	114.6	
DENIS J1048-3956	10 48 14.57	-39 56 07.0	I	4c	92	3.18	9	246.64±1.54	1.07±0.18	247.71±1.55	1530.4±1.3	229.2±0.10	29.3	
LHS 300AB	11 11 13.68	-41 05 32.7	R	4c	65	3.18	12	30.65±1.84	1.65±0.17	32.30±1.85	1249.2±1.4	264.1±0.10	183.3	!
LHS 306	11 31 08.38	-14 57 21.3	R	4c	65	3.18	8	88.20±1.68	1.04±0.15	89.24±1.69	1431.6±1.6	163.2±0.11	76.0	
LHS 346	13 09 20.42	-40 09 27.0	V	4c	71	3.18	9	59.78±1.11	1.97±0.13	61.75±1.12	1233.6±0.9	143.6±0.08	94.7	
ER 2	13 13 09.33	-41 30 39.7	V	4c	49	2.94	8	82.28±1.58	1.30±0.10	83.58±1.58	1027.6±1.8	271.7±0.15	58.3	
LHS 382	14 50 41.22	-16 56 30.8	I	4c	51	3.12	8	19.92±2.25	0.77±0.09	20.69±2.25	1428.7±1.8	244.0±0.14	327.3	!
LHS 406	15 43 18.33	-20 15 32.9	R	5c	61	3.60	10	45.53±1.59	1.75±0.28	47.28±1.61	1161.4±1.3	194.8±0.10	116.4	
LHS 423	16 35 40.40	-30 51 20.2	V	4c	53	3.01	12	49.35±2.93	2.04±0.23	51.39±2.94	1158.2±2.1	223.6±0.20	106.8	
LHS 440	17 18 25.58	-43 26 37.6	R	4s	85	2.94	9	35.19±2.14	1.71±0.47	36.90±2.19	1080.4±2.2	233.8±0.23	138.8	
LTT 6933	17 28 07.33	-62 27 14.2	R	4s	67	2.72	10	59.37±1.50	1.74±0.16	61.11±1.51	959.3±1.6	197.4±0.18	74.4	!
GJ 1226A	18 20 57.18	-01 02 58.0	I	4c	59	3.11	10	37.31±5.27	1.47±0.17	38.78±5.27	1091.6±4.4	207.8±0.45	133.4	!
GJ 1226B	18 20 57.18	-01 02 58.0	I	4c	59	3.11	10	26.27±6.14	1.47±0.17	27.74±6.14	1095.9±5.2	208.3±0.52	187.3	!
LHS 475	19 20 54.26	-82 33 16.1	V	4c+	66	3.75	8	76.46±2.00	1.88±0.33	78.34±2.03	1267.0±1.7	164.6±0.13	76.7	
GJ 1252	20 27 42.07	-56 27 25.2	R	4c	87	2.87	12	48.13±2.13	2.40±0.18	50.53±2.14	1298.7±2.8	161.3±0.22	121.8	
GJ 1251	20 28 03.75	-76 40 15.9	R	4c	68	2.95	7	76.96±2.24	2.06±0.17	79.02±2.25	1426.6±2.2	149.6±0.17	85.6	
LHS 510	21 30 47.67	-40 42 29.5	R	4c	56	3.11	8	82.44±2.52	1.16±0.14	83.60±2.52	1723.9±2.4	143.1±0.16	97.7	
LHS 512	21 38 43.65	-33 39 55.3	V	4c	63	3.13	8	80.34±2.10	1.68±0.06	82.02±2.10	1151.1±1.9	116.7±0.18	66.5	
LHS 521	22 27 59.21	-30 09 32.8	R	4c	68	3.15	11	20.60±1.59	1.00±0.07	21.60±1.59	1008.8±2.2	136.8±0.24	221.4	

Table 2—Continued

Name	RA	DEC	Filt	Nsea	Nfrm	Years	Nref	$\pi(\text{rel})$	$\pi(\text{corr})$	$\pi(\text{abs})$	$\mu$	P.A.	$V_{tan}$	Note
(1)	(J2000.0)		(3)	(4)	(5)	(6)	(7)	(mas)	(mas)	(mas)	(mas/yr)	(deg)	(km/s)	(14)
GJ 1281	23 10 42.16	-19 13 34.9	V	4c	62	3.12	8	40.15±2.31	0.99±0.06	41.14±2.31	1428.1±2.5	178.2±0.15	164.5	
LHS 539	23 15 51.61	-37 33 30.6	R	4c	54	2.89	8	51.93±2.01	0.92±0.07	52.85±2.01	1311.2±3.0	78.4±0.22	117.6	
LHS 547	23 36 52.31	-36 28 51.8	V	4c+	53	2.88	7	85.17±2.03	1.06±0.05	86.23±2.03	1168.9±2.2	87.0±0.16	64.3	
Revised Parallaxes														
GJ 545	14 20 07.36	-09 37 13.4	V	4c	49	3.16	9	71.02±1.38	0.50±0.03	71.52±1.38	1020.7±1.2	216.8±0.14	67.6	!
GJ 754	19 20 47.98	-45 33 29.7	V	5c	121	4.06	9	166.76±1.52	2.27±0.32	169.03±1.55	2960.7±1.1	167.5±0.03	83.0	!
LHS 500	20 55 37.12	-14 03 54.8	V	4c	70	3.00	9	81.07±1.54	0.88±0.05	81.95±1.54	1490.4±1.4	108.1±0.10	86.2	!
LHS 501	20 55 37.76	-14 02 08.1	V	4c	70	3.00	9	76.71±1.49	0.88±0.05	77.59±1.49	1492.3±1.4	108.0±0.09	91.2	!
Parallax Calibration Stars														
LHS 1731	05 03 20.08	-17 22 25.0	V	5c	84	3.72	9	107.53±2.15	1.17±0.11	108.70±2.15	495.9±1.5	207.8±0.34	21.6	
LHS 1777	05 42 12.70	-05 27 55.6	I	4c	45	2.70	7	76.22±1.77	3.50±0.65	79.72±1.89	959.0±2.2	351.2±0.21	57.0	
GJ 440	11 45 42.93	-64 50 29.7	V	4c	93	3.23	10	213.41±2.03	1.66±0.19	215.07±2.04	2698.5±2.0	97.6±0.07	59.5	
GJ 465	12 24 52.49	-18 14 32.2	V	4c	61	3.16	6	108.45±2.44	1.82±0.29	110.27±2.46	2552.6±1.9	154.4±0.08	109.7	
Proxima Cen	14 29 43.02	-62 40 46.7	V	5s	86	3.38	8	772.33±2.05	1.92±0.38	774.25±2.08	3856.0±2.3	281.6±0.05	23.6	!
GJ 555	14 34 16.82	-12 31 10.2	V	4s	69	3.39	8	157.72±2.62	0.74±0.11	158.46±2.62	691.3±2.2	330.3±0.35	20.7	
GJ 581	15 19 26.83	-07 43 20.3	V	4c	122	2.95	8	153.50±2.62	1.16±0.11	154.66±2.62	1222.4±2.8	265.7±0.20	37.5	

Note. — Stars with exclamation mark are discussed in the section 6.3.

Table 3.

Name1 (1)	Name2 (2)	$V$ (3)	$R$ (4)	$I$ (5)	# (6)	Refs (7)	$J$ (8)	$H$ (9)	$K_s$ (10)	Spect. (11)	Refs (12)
GJ 1025	LHS 130	13.35	12.08	10.52	2		9.04	8.49	8.22	M3.5 V	6
GJ 1050	LHS 157	11.79	10.68	9.35	1		8.06	7.54	7.31	M3.5 V	6
LHS 158	L 298-71	13.64	12.66	11.60	2		10.43	9.94	9.73	....	
GJ 1068	LHS 22	13.62	12.21	10.44	2		8.75	8.21	7.90	M4.5 V	6
LHS 193 A		11.66	10.85	10.09	3		9.18	8.55	8.43	....	
LHS 193 B		17.66	17.03	16.08	3		15.98C	15.79C	15.29C	....	
LHS 225 A		12.87	11.85	10.51	1		8.61JD	8.07JD	7.87JD	....	
LHS 225 B		13.02	11.99	10.63	1		....	....	....	....	
GJ 1118	LHS 258	13.79	12.56	10.95	2		9.41	8.86	8.59	M3.0 V	6
GJ 1123	LHS 263	13.16	11.86	10.16	3		8.33	7.77	7.45	M4.5 V	8
GJ 1128	LHS 271	12.74	11.39	9.65	3		7.95	7.39	7.04	M4.5 V	8
GJ 1129	LHS 273	12.39	11.20	9.64	2		8.12	7.54	7.26	M3.5 V	8
WT 248		14.52	13.40	11.95	2	9	10.56	10.10	9.87	M3.0 V	8
LHS 281	GJ 1132	13.49	12.26	10.69	2		9.25	8.67	8.32	M3.5 V	6
WT 1827		15.11	13.57	11.59	2	9	9.67	9.10	8.73	....	
DENI1048-3956		17.39	15.06	12.57	3		9.54	8.91	8.45	M8.5 V	4
LHS 300 A	L 395-13	13.18	12.28	11.49	1		10.48J	10.01J	9.80J	K4.0 VJ	3
LHS 300 B		17.25	16.62	15.70	1		....	....	....	....	
LHS 306		14.19	12.80	11.05	2		9.36	8.76	8.50	M4.5 V	6
LHS 346		12.86	11.73	10.24	2		8.79	8.24	7.99	M3.5 V	6
ER2		12.91	11.61	9.96	1	9	8.29	7.68	7.41	....	
LHS 382		15.30	14.61	13.17	2	10	11.85	11.38	11.11	....	
LHS 406	GJ 2116	13.06	12.07	10.93	2		9.78	9.23	9.02	M1.0 V	3
LHS 423	L 555-14	12.66	11.58	10.16	1		8.89	8.36	8.08	M3.0 V	6

Table 3—Continued

Name1 (1)	Name2 (2)	$V$ (3)	$R$ (4)	$I$ (5)	# (6)	Refs (7)	$J$ (8)	$H$ (9)	$K_s$ (10)	Spect. (11)	Refs (12)
LHS 440	L 413-156	12.98	11.98	10.86	2		9.70	9.13	8.95	M1.0 V	3
LTT 6933	LHS 3292	12.74	11.54	9.95	1		8.42D	7.85D	7.57D	....	
GJ 1226 A	LHS 463 A	13.07	11.98	10.56	1		8.75J	8.19J	7.95J	M3.5 VJ	6
GJ 1226 B	LHS 463 B	13.16	12.07	10.63	1		....	....	....	....	
LHS 475	L 22-69	12.68	11.50	10.00	2		8.56	8.00	7.69	M3.0 V	6
GJ 1252	LHS 492	12.20	11.19	9.93	1		8.70	8.16	7.92	M2.5 V	6
GJ 1251	LHS 493	13.96	12.76	11.11	1		9.36	8.88	8.60	M4.5 V	6
LHS 510	L 425-35	13.12	11.92	10.34	1		8.87	8.42	8.13	M1.5 V	6
LHS 512	L 570-29	12.55	11.38	9.89	1		8.44	7.84	7.57	M3.5 V	6
LHS 521		14.68	13.84	13.10	1		12.13	11.66	11.46	....	
GJ 1281	LHS 538	12.45	11.42	10.19	1		8.98	8.46	8.23	M2.5 V	6
LHS 539		14.98	13.66	11.96	2		10.40	9.87	9.59	....	
LHS 547	L 504-27	13.76	12.46	10.79	3		9.19	8.67	8.42	M4.5 V	6
GJ 545	LHS 369	12.84	11.69	10.15	2		8.74	8.19	7.98	M3.5 V	6
GJ 754	LHS 60	12.26	10.93	9.24	1	2	7.66	7.13	6.85	M4.5 V	6
LHS 500	GJ 810 B	14.61	13.19	11.38	1	2	9.72	9.22	8.92	M5.0 V	6
LHS 501	GJ 810 A	12.48	11.22	9.61	1	2	8.12	7.64	7.37	M4.0 V	6
LHS 1731		11.69	10.59	9.16	1	10	7.82	7.24	6.94	M3.0 V	8
LHS 1777		15.29	13.81	11.92	1	5	10.21	9.69	9.37	M5.5 V	6
GJ 440	LHS 43	11.50	11.33	11.19	3	1	11.19	11.13	11.10	DQ6.0	11
GJ 465	LHS 45	11.27	10.23	8.92	1	2	7.73	7.25	6.95	M2.0 V	6
Proxima Cen	LHS 49	...	...	...	...	2	5.36	4.84	4.38	M5.5 V	6
GJ 555	LHS 2945	11.30	10.05	8.43	1	10	6.84	6.26	5.94	M3.5 V	8
GJ 754	LHS 394	10.55	9.44	8.04	2	2	6.71	6.10	5.84	M3.0 V	6

Table 3—Continued

Name1	Name2	<i>V</i>	<i>R</i>	<i>I</i>	#	Refs	<i>J</i>	<i>H</i>	<i>K<sub>s</sub></i>	Spect.	Refs
(1)	(2)	(3)	(4)	(5)	(6)	(7)	(8)	(9)	(10)	(11)	(12)

Note. — C: affected by confusion with another nearby source; D: affected by a nearby diffraction spike; J: joined (combined) photometry

References. — (1): Bergeron, Leggett, & Ruiz 2001; (2): Bessel 1990; (3): Bidelman 1985; (4): Henry et al. 2004; (5): Harrington et al. 1993; (6): Hawley, Gizis, & Reid 1996; (7): Henry, Kirkpatrick, & Simons 1994; (8): Henry et al. 2002; (9): Patterson, Ianna, & Begam 1998; (10): Weis 1996; (11): McCook & Sion 1999.